American Journal of Modern Physics
2018; 7(4): 136-165
http://www.sciencepublishinggroup.com/j/ajmp
doi: 10.11648/j.ajmp.20180704.13
ISSN: 2326-8867 (Print); ISSN: 2326-8891 (Online)

Effects of Donor Size and Heavy Doping on Optical, Electrical and Thermoelectric Properties of Various Degenerate Donor-Silicon Systems at Low Temperatures

Huynh Van Cong

Department of Physics, Laboratory of Mathematics and Physics, University of Perpignan, Perpignan, France

Email address:
huynh@univ-perp.fr, huynhvc@outlook.fr

To cite this article:
Huynh Van Cong, Effects of Donor Size and Heavy Doping on Optical, Electrical and Thermoelectric Properties of Various Degenerate Donor-Silicon Systems at Low Temperatures. *American Journal of Modern Physics.* Vol. 7, No. 4, 2018, pp. 136-165.
doi: 10.11648/j.ajmp.20180704.13

Received: July 1, 2018; **Accepted**: July 13, 2018; **Published**: August 8, 2018

Abstract: In various degenerate donor-silicon systems, taking into account the effects of donor size and heavy doping and using an effective autocorrelation function for the potential fluctuations expressed in terms of the Heisenberg uncertainty relation and also an expression for the Gaussian average of $\mathbb{E}_k^{a-\frac{1}{2}}$, $a \geq 1$ $\mathbb{E}_k$ being the kinetic energy of the electron, calculated by the Kane integration method (KIM), we investigated the density of states, the optical absorption coefficient and the electrical conductivity, noting that this average expression calculated by the KIM was found to be equivalent to that obtained by the Feynman path-integral method. Then, those results were expressed in terms of $\mathbb{E}^{a-(1/2)}$ for total electron energy $\mathbb{E} \geq 0$, vanished at the conduction-band edge: $\mathbb{E} = 0$, and for $\mathbb{E} \leq 0$ exhibited their exponential tails, going to zero as $\mathbb{E} \to -0$ and $-\infty$, and presenting the maxima, in good accordance with an asymptotic form for exponential conduction-band tail obtained by Halperin and Lax, using the minimum counting methods. Further, in degenerate d-Si systems at low temperatures, using an expression for the average of $\mathbb{E}^p$, $p \geq 3/2$, calculated using the Fermi-Dirac distribution function, we determined the mobility, electrical conductivity, resistivity, Hall factor, Hall coefficient, Hall mobility, thermal conductivity, diffusion coefficient, absolute thermoelectric power, Thomson coefficient, Peltier coefficient, Seebeck thermoelectric potential, and finally dimensionless figure of merit, which were also compared with experimental and theoretical results, suggesting a satisfactory description given for our obtained results.

Keywords: Donor Size, Heavy Doping, Electrical Conductivity, Hall Effect, Diffusion Coefficient

1. Introduction

Donor (acceptor)-silicon d (a)-Si system at a given temperature T, doped with a given d (a)-density N, assuming that all the impurities are ionized, is the base material of modern semiconductor devices [1-6]. Then, due to the Fermi-Dirac statistics, there are three cases may be classified as: non-degenerate ($T >> T_D$ and $N << N_c$), moderately degenerate ($T > T_D$ and $N >> N_c$) and degenerate ($T << T_D$ and $N >> N_c$)-cases, T_D and N_c being respectively the degenerate temperature defined in Eq. (15) and critical impurity density.

In the present paper, the degenerate d-Si system is considered, noting that all the optical, electrical, and thermoelectric properties given in the degenerate a-Si system can also be investigated by a same treatment.

So, in the degenerate d-Si system, a good knowledge of: (i) energy-band structure parameters such as: the reduced band gap [7-12], $N_{c(d)}$ [11, 12] and effective donor ionization energy [13], (ii) exponential conduction-band tails [14-25] and Fermi energy [26-28], and finally (iii) optical [29-48], electrical [49-69], and thermoelectric [58, 61, 68, 69] properties, due to the effects of donor size [11, 12, 42, 43, 53], heavy doping [14, 17-30, 34, 35, 48-68], and low T [49, 58], is thus necessary for designing new devices and also understanding their performance.

In Section 2, we studied the effects of donor size [or compression (dilatation)], temperature, and heavy doping on the energy-band-structure parameters. At T = 0 K, with

increasing values of donor radius r_d, since the effective dielectric constant $\varepsilon_n(r_d)$ decreases, due to the donor-size effect, the effective donor ionization $\mathbb{E}_{do}(r_d)$, unperturbed intrinsic band gap $\mathbb{E}_{go}(r_d)$, and critical donor density $N_{c(d)}$ increase, as seen in Table 1. Then, for a given r_d, the effective intrinsic band gap $\mathbb{E}_{gi}(r_d, T)$, due to the T-effect, decreases with increasing T, as given in Eq. (3). Finally, due to the heavy doping effect (HDE), for a given r_d, the effective electron mass $m_n^{HDE}(N, r_d)$ increases with increasing N, as given in Eq. (8), and for given r_d and T, the reduced band gap $\mathbb{E}_{gn2}(N, T, r_d)$ decreases with increasing N, as given in Eq. (10).

In Section 3, the effective autocorrelation function for potential fluctuations, W_n, was determined and in Eq. (B.6) the appendix B, being a central result of the present paper, as noted in Eq. (20). It was suggested that $W_n(\mathbb{E} \to \pm\infty) \to \eta_n^2$, $\mathbb{E}$ and η_n being respectively the total electron energy and the energy parameter characteristic of the conduction-band tail states, and $W_n(\mathbb{E} \to \pm 0) \to 0$. Therefore, the density of states, the optical absorption coefficient and the electrical conductivity, being proportional to our result (20), vanished at the conduction-band edge $\mathbb{E} = 0$, as given in Eqs. (23, 26). Those results were also compared with other theoretical results, obtained at $-\mathbb{E} = 0$, in the small time approximation [21, 29, 30] and in the full ground-state case and deep-tail approximation [21], which were found to be constant, being not correct, as discussed also in Eq. (26). Then, for $\mathbb{E} \leq 0$, their exponential tails were obtained in Figures 1, 4 and 7, in which they increased with increasing r_d for a given value of $-\mathbb{E}$, due to the donor-size effect, and further they went to zero as $\mathbb{E} \to -0$ and $-\infty$ and presented the maxima, being found to be in good accordance with an asymptotic form for exponential conduction-band tail, obtained by Halperin and Lax [19], using the minimum counting methods.

In Section 4, we determined the average of $\mathbb{E}^p$ at low temperature T ($T << T_D$), using the Fermi-Dirac distribution function (FDDF), $\langle \mathbb{E}^p \rangle_{FDDF} \equiv G_p(\mathbb{E}_{Fn}) \times \mathbb{E}_{Fn}^p$, for $p \geq 3/2$, as given in Eq. (34) and Table 3, $\mathbb{E}_{Fn}$ being the Fermi energy determined in Eq. (A10) of the Appendix C.

In Section V, we determined the critical donor density, as given in Table 1, suggesting that its numerical results are in good agreement with the corresponding data given in Ref. 12, and it increases with increasing r_d, due to the donor-size effect [12]. Then, for $\mathbb{E} \leq 0$, the exponential band-tail behaviors were investigated and reported in Table 4, and also in Figures 1 and 2a (b).

In Section 6, various optical functions were determined in band-to-band transitions ($\mathbb{E} \geq 0$) as found in Figs. 3a, 3b, 3c, being compared with other theoretical and experimental works [33-35, 38, 44-48], and also the exponential optical absorption-coefficient tail behaviors were investigated when $\mathbb{E} \leq 0$, as seen in Table 7, and Figures 4 and 5a (b).

In Section 7, for $\mathbb{E} \geq 0$, using the functions G_p obtained at low T, given in Table 3, we determined various electric functions as those given in Tables 10-13, in good accordance with the corresponding experimental results [50, 53, 54, 56-61], and for $\mathbb{E} \leq 0$, we also studied the exponential conductivity-tail behaviors, as those given in Tables 14 and Figures 7, 8a (b).

In Section 8, for $\mathbb{E} \geq 0$, using also the function G_p, we studied various thermoelectric functions, and reported their numerical results in Table 15 and Figures 9a, 9b, 9c, 9d, 9e, and 9f, noting that for $\mathbb{E} \leq 0$ we could also study the exponential thermoelectric function-tail behaviors by a same treatment, as those obtained in Sections 5-7.

Finally, some concluding remarks were given and discussed in Section 9.

2. Energy-Band-Structure Parameters

Here, we study the effects of donor size, temperature, and heavy doping on the energy-band-structure parameters.

2.1. Donor-Size Effect

In donor-Si systems at T=0 K, since the d-radius, r_d, in tetrahedral covalent bonds is usually either larger (or smaller) than the Si atom-radius, r_o, assuming that in the P-Si system $r_P = r_o = 0.117$ nm, with nm $= 10^{-9}$m, a local mechanical strain (or deformation potential-or-strained energy) is induced, according to a compression (dilation) for $r_d > r_o$ ($r_d < r_o$), respectively, or to the donor size (r_d)-effect. In the Appendix A of our recent paper [12], basing on an effective Bohr model, such a compression (dilation) occurring in various donor (d)-Si systems was investigated, suggesting that the effective dielectric constant, $\varepsilon_n(r_d)$, decreases with increasing r_d. This donor size (r_d)-effect affects the changes in all the energy-band-structure parameters or the electronic properties of various donor-Si systems, expressed in terms of $\varepsilon_n(r_d)$, as those investigated in our recent paper [12], noting that $\varepsilon_n(r_P) = 11.4$. In particular, the changes in the unperturbed intrinsic band gap, $\mathbb{E}_{go}(r_P) = 1170$ meV, effective donor ionization energy, $\mathbb{E}_{do}(r_P) = 33.58$ meV, and critical donor (P)-density, $N_{c(P)} = 3.5 \times 10^{18}$ cm^{-3}, of the P-Si system at 0 K, are obtained in an effective Bohr model, as [12]

$$\mathbb{E}_{go}(r_d) - \mathbb{E}_{go}(r_P) = \mathbb{E}_{do}(r_d) - \mathbb{E}_{do}(r_P) = \mathbb{E}_{do}(r_P) \times \left[\left(\frac{\varepsilon_n(r_P)}{\varepsilon_n(r_d)}\right)^2 - 1\right],$$

and in a simple generalized Mott model, by [12]

$$N_{c(r_d)} = N_{c(P)} \times \left(\frac{\varepsilon_n(r_P)}{\varepsilon_n(r_d)}\right)^3.$$

Therefore, with increasing r_d, the effective dielectric constant $\varepsilon_n(r_d)$ decreases, implying thus that $\mathbb{E}_{go}(r_d)$, $\mathbb{E}_{do}(r_d)$ and $N_{c(r_d)}$ increase. Those changes, given in our previous paper [12], are now reported in the following Table 1, in which the numerical results of critical donor density, due to the exponential band tail (EBT)-effect, $N_{c(d),\mathscr{b}}^{EBT}$, being obtained in the next Section V, are also included for a comparison. Here, $\mathscr{b}$ is normally equal to 1, but it will be chosen as: $\mathscr{b} = \mathscr{b}_o = 1.0028637416$, so that the obtained

results of $N_{c(r_d),\mathscr{E}_o}^{EBT}$ would be more accurate.

Table 1. *The following values of r_d, ε_n, a_{no}, $E_{go}(r_d)$, and $N_{c(d)}$-data, given in our previous paper [12], are now reported in this TABLE, in which we also include the numerical results of $N_{c(d),\mathscr{E}}^{EBT}$, where $\mathscr{E} = 1$ or $\mathscr{E}_o = 1.0028637416$, calculated using Eqs. (41, 42), and their absolute relative errors defined by: $|RE| \equiv \left|1 - \frac{N_{c(d),\mathscr{E}}^{EBT}}{N_{c(d)}}\right|$. Here, $nm \equiv 10^{-9}\ m$.*

Donor	**Sb**	**P**	**As**	**Bi**	**Ti**	**Te**	**Se**	**S**
r_d (nm)	0.1131	0.1170	0.1277	0.1292	0.1424	0.1546	0.1621	0.1628
$\varepsilon_n(r_d)$	12.02	11.40	8.47	7.95	4.71	3.26	2.71	2.67
$\mathbb{E}_{do}(r_d)$ (meV)	30.18	33.58	60.82	69	197	411	593	613
$\mathbb{E}_{go}(r_d)$ (meV)	1167	1170	1197	1205	1333	1547	1729	1749
$N_{c(d)}$ (10^{18} cm^{-3})	3	3.52	8.58	10.37	50	150.74	261.24	274.57
$N_{c(d),\mathscr{E}_o}^{EBT}$ (10^{18} cm^{-3})	3.000003	3.520005	8.579950	10.368890	49.999984	150.738620	261.241940	274.568990
$\|RE\|$	1.1×10^{-6}	1.3×10^{-6}	6.1×10^{-6}	1.1×10^{-4}	3.1×10^{-7}	4.1×10^{-6}	2.1×10^{-7}	2.2×10^{-10}
$N_{c(d),1}^{EBT}$ (10^{18} cm^{-3})	2.991440	3.509950	8.555450	10.339280	49.857210	150.308180	260.495950	273.784950
$\|RE\|$	2.8×10^{-3}	2.8×10^{-3}	2.9×10^{-3}	3.0×10^{-3}	2.9×10^{-3}	2.8×10^{-3}	2.8×10^{-3}	2.8×10^{-3}

The underlined $|RE|$-value is the maximal one, indicating that $N_{c(d),\mathscr{E}_o}^{EBT} \cong N_{c(d)}$.

Moreover, it should be noted that in donor-Si systems such the $\mathbb{E}_{gi}(r_d, 300\ K)$-increase with increasing r_d observed in Table I, $\mathbb{E}_{gi}$ being the effective intrinsic band gap given in next Eq. (3), well agrees with a result obtained recently by Ding et al. [42]. In fact, in their study of the optical properties of isolated silicon nano-crystals (nc-Si) with the size of $2r_{nc-Si} = 4.2$ nm ($\gg 2r_P = 2 \times 0.117$ nm) embedded in a SiO_2 matrix, they showed that $\mathbb{E}_{gi}(r_{nc-Si}, 300\ K) = 1.79\ eV \gg \mathbb{E}_{gi}(r_P, 300\ K) = 1.12\ eV$ given in the bulk crystalline Si at room temperature, being also due to the size effect ($r_{nc-Si} \gg r_P$).

Now, the effective Bohr radius can be defined by

$$a_B(r_d, m^*) \equiv \frac{m_o}{m^*} \times \varepsilon_n(r_d) \times 5.3\ \text{nm}. \quad (1)$$

In Eq. (1), m^* is the effective electron mass given in the Si, being equal to: (i) the effective mass $m_n = 0.3216 \times m_o$, m_o being the free electron mass, defined for the calculation of $m_n^{HDE}(N)$, as determined in next Eq. (8), due to the heavy doping effect (HDE), (ii) the reduced effective mass: $m_r = \frac{m_n \times m_p}{m_n + m_p} \times m_o = 0.171 \times m_o$, for the optical absorption-coefficient calculation, where $m_p = 0.3664 \times m_o$ is the effective hole mass in the silicon [12], (iii) $m_n^{HDE}(N)$, given in next Eq. (8), for the determination of the density of states, as given in Section 5, and finally (iv) the conductivity effective mass: $m_{cond.} = 0.26 \times m_o$ for the electrical conductivity calculation [6], as used in Section 7.

Then, in the degenerate case ($N > N_{c(d)}$), denoting the Fermi wave number by: $k_{Fn}(N) \equiv (3\pi^2 N/g_c)^{1/3}$, where $g_c = 3$ is the effective average number of equivalent conduction-band edges [11, 12], the effective Wigner-Seitz radius r_{sn} characteristic of the interactions is defined by

$$\gamma \times r_{sn}(N, r_d, m^*) \equiv \frac{k_{Fn}^{-1}}{a_B} < 1, \quad (2)$$

being proportional to $N^{-1/3}$. Here, $\gamma = (4/9\pi)^{1/3}$, and k_{Fn}^{-1} means the averaged distance between ionized donors.

2.2. Temperature Effect

Here, in d-Si systems, being inspired from recent works by Pässler [8, 9], we can propose an accurate expression for the effective intrinsic band gap as a function of r_d and T, as

$$\mathbb{E}_{gi}(T, r_d) \simeq \mathbb{E}_{go}(r_d) - 0.071\ (\text{eV}) \times \left\{\left[1 + \left(\frac{2T}{440.6913\ K}\right)^{2.201}\right]^{\frac{1}{2.201}} - 1\right\}. \quad (3)$$

For example, in the (P, S)-Si systems, for $0 \le T\ (K) \le 3500$, the absolute maximal relative errors of $\mathbb{E}_{gi}$ are equal to: 0.22%, 0.15%, respectively, calculated using the accurate complicated results given by Pässler [9].

2.3. Heavy Doping Effect (HDE)

HDE on m_n

Now, using Eq. (2) for $r_{sn}(N, r_d, m^* = m_n)$, the ratio of the inverse effective screening length k_{sn} to Fermi wave number k_{Fn} at 0 K is defined by [12]

$$R_{sn}(N, r_d) \equiv \frac{k_{sn}}{k_{Fn}} = \frac{k_{Fn}^{-1}}{k_{sn}^{-1}} = R_{snWS} + [R_{snTF} - R_{snWS}]e^{-r_{sn}} < 1. \quad (4)$$

It is noted that, in the very high electron-density limit [or in the Thomas-Fermi (TF)-approximation], R_{sn} is reduced to

$$R_{snTF}(N, r_d) \equiv \frac{k_{snTF}}{k_{Fn}} = \frac{k_{Fn}^{-1}}{k_{snTF}^{-1}} = \sqrt{\frac{4\gamma r_{sn}}{\pi}} \ll 1, \quad (5)$$

being proportional to $N^{-1/6}$. It should be noted that the effective screening length k_{snTF}^{-1} is very larger than the averaged distance between ionized donors k_{Fn}^{-1} (i.e., this is the TF-condition given in the very degenerate case, $N \gg$

$N_{c(d)}$), and in the very low electron-density limit [or in the Wigner-Seitz (WS)-approximation], R_{sn} is reduced to

$$R_{snWS}(N, r_d) \equiv \frac{k_{snWS}}{k_{Fn}} = \frac{3}{2\pi} - \gamma \frac{d[r_{sn}^2 \times \mathbb{E}_{CE}]}{dr_{sn}}, \gamma = (4/9\pi)^{1/3}. \quad (6)$$

Here, when the relative spin polarization ζ is equal to zero (paramagnetic state), $\mathbb{E}_{CE}$ means the majority-electron correlation energy (CE), determined by as [11, 12]

$$\mathbb{E}_{CE}(N, r_d) = \frac{-0.87553}{0.0908+r_{sn}} + \frac{\left[\frac{0.87553}{0.0908+r_{sn}} + a_P \times Ln(r_{sn}) + b_P\right]}{1+0.03847728 \times r_{sn}^{1.67378876}}, \quad (7)$$

where $a_P = 2[1 - \mathrm{Ln}(2)]/\pi^2$ and $b_P = -0.093288$. Then, due to such the HDE, the effective electron mass can be approximated by [11, 12]

$$m_n^{HDE}(N, r_d) = \left(1 + \frac{4\gamma \times r_{sn}}{3\pi\left[1+R_{sn}^2\right]^2}\right) \times m_n. \quad (8)$$

HDE on $\mathbb{E}_{gi}$

In the degenerate case, the optical band gap is defined by

$$\mathbb{E}_{gn1}(N, T, r_d) \equiv \mathbb{E}_{gn2}(N, T, r_d) + \mathbb{E}_{Fn}(N, T), \quad (9)$$

where $\mathbb{E}_{Fn}$ is the Fermi energy determined at any N and T in Eq. (C.1) of the Appendix C, with an accuracy equal to: 2.11×10^{-4}, and $\mathbb{E}_{gn2}$ is the reduced band gap defined as

$$\mathbb{E}_{gn2}(N, T, r_d) \equiv \mathbb{E}_{gi}(T, r_d) - BGN(N, r_d), \quad (10)$$

where the intrinsic band gap $\mathbb{E}_{gi}(T, r_d)$ is determined in Eq. (3) and the band gap narrowing (BGN) is determined below.

In our recent paper [12], an accurate formula for the BGN was investigated, being expressed in the following spin-polarized chemical potential-energy contributions, as:
the exchange energy of an effective electron gas,
the majority-electron correlation energy of an effective electron gas,

(iii) the minority-hole correlation energy,

(iv) the majority electron-ionized donor interaction screened Coulomb potential energy, and finally

(v) the minority hole-ionized donor interaction screened Coulomb potential energy.

It should be noted that the two last contributions (iv) and (v) are found to be the most important ones. Therefore, an approximate form for the BGN can be proposed by

$$BGN(N, r_d) \simeq C_n \times \left(\frac{N}{10^{18}\ cm^{-3}}\right)^{1/2} \times \left(\frac{11.4}{\varepsilon_n(r_d)}\right)^{1/2} \times \left(\frac{m_n}{m_n^{HDE}(N, r_d)}\right)^{1/2} \times \left[1 + \left(\frac{m_n^{HDE}(N, r_d)}{m_p}\right)^{1/2}\right], \quad (11)$$

which is a very simplified form compared with our previous complicated expression for BGN [12].

Here, the values of effective dielectric constant $\varepsilon_n(r_d)$ are given in Table 1 and the electron effective mass $m_n^{HDE}(N, r_d)$, due to the heavy doping effect, is determined in Eq. (8). Further, the empirical parameter $C_n = 8.5 \times 10^{-3}$ (eV) has been chosen so that the absolute maximal relative error |MRE| of our result (9), calculated using the optical band-gap ($\mathbb{E}_{gn1}$)-data for P-Si systems at 20 K obtained by Wagner, [7] are found to be minimized.

In a degenerate P-Si system, with use of the next Eq. (43), obtained for the definition of effective density of free electrons given in the conduction band, $N^* \simeq N - N_{c(P)}$, where the value of $N_{c(P)}$ is given in Table I, our present results of $\mathbb{E}_{gn1}(N^*, T = 20\ K, r_P)$, computed using Eqs. (9, 11), and their absolute relative errors |REs|, calculated using the $\mathbb{E}_{gn1}$-data at 20 K [12], are obtained and reported in Table 2, in which our previous accurate $\mathbb{E}_{gn1}(N^*)$-results and their |REs| are also included [12], for a comparison.

Table 2. *Numerical results of optical band gap at T=20 K, $\mathbb{E}_{gn1}(N^*)$, expressed in eV, being investigated in our recent paper [12], and determined in Eq. (9), and finally their absolute relative errors |RE|, calculated using the $\mathbb{E}_{gn1}$-data [7].*

N (10^{18} cm^{-3})	4	8.5	15	50	80	150
$\mathbb{E}_{gn1}$-data	1.138	1.133	1.129	1.131	1.132	1.133
$\mathbb{E}_{gn1}(N^*)$ [12]	1.149	1.138	1.134	1.126	1.123	1.119
|RE| (%)	0.9	0.5	0.5	0.4	0.8	1.2
$\mathbb{E}_{gn1}(N^*)$, Eq. (9)	1.160	1.147	1.139	1.123	1.118	1.113
|RE| (%)	1.9	1.3	0.9	0.7	1.2	1.7

The underlined |RE|-value is the maximal one.

This table indicates that the maximal value of |REs|, obtained from our present $\mathbb{E}_{gn1}(N^*)$-result, is found to be equal to 1.7%, which can be compared with that equal to 1.2% obtained from our previous $\mathbb{E}_{gn1}(N^*)$-result [12].

HDE conditions

Finally, in degenerate d-Si systems, the energy parameter η_n, being characteristic of the exponential conduction-band tail, is determined in Eq. (B.4) of the Appendix B as

$$\eta_n(N, r_d) \equiv \sqrt{2\pi N} \times q^2 k_{sn}^{-1/2} \varepsilon_n^{-1}, \quad (12)$$

where $k_{sn}^{-1/2}$ is determined in Eq. (4). Moreover, in highly degenerate case ($N \gg N_{c(d)}$) or in the Thomas-Fermi approximation, $k_{sn}^{-1/2} \simeq k_{snTF}^{-1/2}$, determined in Eq. (5), η_n is found to be proportional to $N^{5/12}$.

Then, from Eq. (12) and next Eq. (15), we can obtain another heavy doping condition as

$$\frac{\eta_n}{\mathbb{E}_{Fno}} < 1, \quad (13)$$

being proportional to $N^{-1/4}$ in this highly degenerate case.

In summary, in the highly degenerate case ($N \gg N_{c(d)}$) and from Eqs. (2, 4, 13), one has

$$\frac{k_{Fn}^{-1}}{a_B} < \frac{\eta_n}{\mathbb{E}_{Fno}} < \frac{k_{Fn}^{-1}}{k_{sn}^{-1}} < 1, \quad (14)$$

where $\mathbb{E}_{Fno}$ is the Fermi energy at 0 K, defined by

$$\mathbb{E}_{Fno}(N) \equiv \frac{\hbar^2 \times k_{Fn}^2(N)}{2 \times m^*}. \quad (15)$$

In Eq. (15), m^* is the electron effective mass, defined in Eq. (1), and in this highly degenerate case one has a low T-condition as: $T \ll T_D \equiv \mathbb{E}_{Fno}(N)/k_B$, T_D and k_B being the

degeneracy temperature and the Boltzmann's constant, respectively.

3. Effective Autocorrelation Function and its Applications

In the degenerate d-Si systems, the total screened Coulomb impurity potential energy due to the attractive interaction between an electron charge, $-q$, at position $\vec{r}$ and an ionized donor charge: $+q$ at position $\overrightarrow{R_j}$ randomly distributed throughout the Si crystal, is defined by

$$V(r) \equiv \sum_{j=1}^{\mathcal{N}} v_j(r) + V_o, \tag{16}$$

where $\mathcal{N}$ is the total number of ionized donors, V_o is a constant potential energy, and $v_j(r)$ is a screened Coulomb potential energy for each d-Si system, defined as

$$v_j(r) \equiv -\frac{q^2 \times \exp(-k_{sn} \times |\vec{r} - \overrightarrow{R_j}|)}{\varepsilon_n \times |\vec{r} - \overrightarrow{R_j}|}. \tag{17}$$

Further, using a Fourier transform, the v_j-representation in wave vector $\vec{k}$-espace is given by

$$v_j(\vec{k}) = -\frac{q^2}{\varepsilon_n} \times \frac{4\pi}{\Omega} \times \frac{1}{k^2 + k_{sn}^2}, \tag{18}$$

where Ω is the total Si-crystal volume and k_{sn} is the inverse screening length determined in Eq. (4). Moreover, in Eqs. (16, 17), V_o is defined as a constant so that $\langle V(r) \rangle = 0$, reflecting a charge neutrality, where the notation $\langle ... \rangle$ denotes the configuration average [25, 58]. In fact, from Eq. (17), one has

$$\langle \sum_{j=1}^{\mathcal{N}} v_j(r) \rangle = (\mathcal{N}/\Omega) \int_0^{\infty} v_j(r) \times 4\pi r^2 dr = -4\pi N q^2 k_{sn(sp)}^{-2} \varepsilon_{n(p)}^{-1} \equiv -V_o,\ N \equiv \mathcal{N}/\Omega,$$

indicating that from Eq. (16) one obtains: $\langle V(r) \rangle = 0$.

Therefore, the effective autocorrelation function for potential fluctuations can thus be defined by [25, 58]

$$W_n(|\vec{r} - \vec{r'}|) \equiv \langle V(r)V(r') \rangle \equiv \langle V(r) \rangle \times \langle V(r') \rangle + \langle\langle V(r)V(r') \rangle\rangle = \langle\langle V(r)V(r') \rangle\rangle,$$

where $\langle\langle V(r)V(r') \rangle\rangle$ denotes the effective second-order cumulant, and $\overrightarrow{r(t)}$ and $\overrightarrow{r'(t')}$ are the electron positions at the times t and t', noting that the cumulant is just the average potential energy, which may be absorbed by a redefinition of the zero energy. Then, the expression for W_n is determined in Eq. (B.6) of the Appendix B, as

$$W_n(\nu_n, N, r_d) \equiv \langle V(r)V(r') \rangle = \eta_n^2 \times \exp\left(\frac{-\mathcal{H}_n \times R_{sn}}{2\sqrt{|\nu_n|}}\right). \tag{19}$$

Here, $R_{sn}(N)$ is given in Eq. (4), η_n is determined in Eq. (12), the constant $\mathcal{H}_n$ will be chosen in next Section V as: $\mathcal{H}_n = 5.4370$, such that the determination of the density of electrons localized in the conduction-band tail would be accurate, and finally $\nu_n \equiv \frac{-\mathbb{E}}{\mathbb{E}_{Fno}}$, where $\mathbb{E}$ is the total electron energy and $\mathbb{E}_{Fno}$ is the Fermi energy at 0 K, determined in Eq. (15).

Now, we calculate the ensemble average of the function: $(\mathbb{E} - V)^{a-\frac{1}{2}} \equiv \mathbb{E}_k^{a-\frac{1}{2}}$, for $a \geq 1$, where $\mathbb{E}_k \equiv \frac{\hbar^2 \times k^2}{2 \times m^*}$ is the kinetic energy of the electron and $V(r)$ is determined in Eq. (16), using the two following integration methods, which strongly depend on the effective autocorrelation function for potential fluctuations $W_n(\nu_n, N)$, determined in Eq. (19).

3.1. Kane Integration Method

In heavily doped d-Si systems, the effective Gaussian distribution probability is defined by

$$P(V) \equiv \frac{1}{\sqrt{2\pi W_n}} \times \exp\left[\frac{-V^2}{2W_n}\right].$$

So, in the Kane integration method (KIM), the Gaussian average of $(\mathbb{E} - V)^{a-\frac{1}{2}} \equiv \mathbb{E}_k^{a-\frac{1}{2}}$ is defined by [14]

$$\langle (\mathbb{E} - V)^{a-\frac{1}{2}} \rangle_{KIM} \equiv \langle \mathbb{E}_k^{a-\frac{1}{2}} \rangle_{KIM} = \int_{-\infty}^{\mathbb{E}} (\mathbb{E} - V)^{a-\frac{1}{2}} \times P(V) dV, \text{ for } a \geq 1.$$

Then, by variable changes: $s = (\mathbb{E} - V)/\sqrt{W_n}$ and $x = -\mathbb{E}/\sqrt{W_n}$, and using an identity [15]:

$$\int_0^{\infty} s^{a-\frac{1}{2}} \times \exp(-xs - \frac{s^2}{2}) ds \equiv \Gamma(a + \tfrac{1}{2}) \times \exp(x^2/4) \times D_{-a-\frac{1}{2}}(x),$$

where $D_{-a-\frac{1}{2}}(x)$ is the parabolic cylinder function, $\Gamma(a + \frac{1}{2})$ is the Gamma function, one thus finds

$$\langle \mathbb{E}_k^{a-\frac{1}{2}} \rangle_{KIM} = \frac{\exp(-x^2/4) \times W_n^{\frac{2a-1}{4}}}{\sqrt{2\pi}} \times \Gamma(a + \tfrac{1}{2}) \times D_{-a-\frac{1}{2}}(x). \tag{20}$$

This result (20) will used to study the optical, electrical, and thermoelectric properties of various degenerate d-Si systems, depending on W_n defined in Eq. (19) and the variable x, expressed also in terms of W_n, as

$$x = \frac{-\mathbb{E}}{\sqrt{W_n}} \equiv A_n \times \nu_n \times \exp\left(\frac{\mathcal{H}_n \times R_{sn}}{4\times\sqrt{|\nu_n|}}\right), A_n \equiv \frac{\mathbb{E}_{Fno}}{\eta_n}, \nu_n \equiv \frac{-\mathbb{E}}{\mathbb{E}_{Fno}}, \tag{21}$$

where $\mathbb{E}_{Fno}$ and η_n are determined in Eqs. (15, 12), respectively. Therefore, the effective autocorrelation function for potential fluctuations W_n, defined in Eq. (19), is thus a central result of the present paper.

3.2. Feynman Path-Integral Method

In the Feynman path-integral method (FPIM), the ensemble average of $(\mathbb{E}-V)^{a-\frac{1}{2}}$ is defined by

$$\langle(\mathbb{E}-V)^{a-\frac{1}{2}}\rangle_{FPIM} \equiv \langle\mathbb{E}_k^{a-\frac{1}{2}}\rangle_{FPIM} \equiv \frac{\hbar^{a-\frac{1}{2}}}{2^{3/2}\times\sqrt{2\pi}} \times \frac{\Gamma(a+\frac{1}{2})}{\Gamma(\frac{3}{2})} \times \int_{-\infty}^{\infty}(it)^{-a-\frac{1}{2}} \times \exp\left\{\frac{i\mathbb{E}t}{\hbar} - \frac{\left(t\sqrt{W_n}\right)^2}{2\hbar^2}\right\} dt,\ i^2 = -1,$$

noting that as a=1, $(it)^{-\frac{3}{2}} \times \exp\left\{-\frac{\left(t\sqrt{W_n}\right)^2}{2\hbar^2}\right\}$ is found to be proportional to the averaged Feynman propagator given the dense donors [16].

Then, by variable changes: $t = \frac{\hbar}{\sqrt{W_n}}$ and $x = -\mathbb{E}/\sqrt{W_n}$ and then using an identity [15]:

$$\int_{-\infty}^{\infty}(is)^{-a-\frac{1}{2}} \times \exp\left\{ixs - \frac{s^2}{2}\right\} ds \equiv 2^{3/2} \times \Gamma(3/2) \times \exp(-x^2/4) \times D_{-a-\frac{1}{2}}(x),$$

one finally obtains: $\langle\mathbb{E}_k^{a-\frac{1}{2}}\rangle_{FPIM} \equiv \langle\mathbb{E}_k^{a-\frac{1}{2}}\rangle_{KIM}$, where $\langle\mathbb{E}_k^{a-\frac{1}{2}}\rangle_{KIM}$ is determined in Eq. (20).

In the following, with use of asymptotic forms for $D_{-a-\frac{1}{2}}(x)$ [15], those given for $\langle(\mathbb{E}-V)^{a-\frac{1}{2}}\rangle_{KIM}$ will be obtained in the two cases: $\mathbb{E} \geq 0$ and $\mathbb{E} \leq 0$.

$\mathbb{E} \geq 0$-case

As $\mathbb{E} \to +\infty$, from Eq. (21), one has: $\nu_n \to -\infty$ and $x \to -\infty$. In this case, one gets [15]:

$$D_{-a-\frac{1}{2}}(x \to -\infty) \approx \frac{\sqrt{2\pi}}{\Gamma(a+\frac{1}{2})} \times e^{\frac{x^2}{4}} \times (-x)^{a-\frac{1}{2}}.$$

Therefore, Eq. (20) becomes

$$\langle\mathbb{E}_k^{a-\frac{1}{2}}\rangle_{KIM} \approx \mathbb{E}^{a-\frac{1}{2}}. \tag{22}$$

Further, as $\mathbb{E} \to +0$, from Eq. (21), one has: $\nu_n \to -0$ and $x \to -\infty$. Therefore, one gets [15]

$$D_{-a-\frac{1}{2}}(x \to -\infty) \simeq \beta(a) \times \exp\left((\sqrt{a} + \frac{1}{16a^{\frac{3}{2}}})x - \frac{x^2}{16a} + \frac{x^3}{24\sqrt{a}}\right) \to 0,\ \beta(a) = \frac{\sqrt{\pi}}{2^{\frac{2a+1}{4}}\Gamma(\frac{a}{2}+\frac{3}{4})].$$

Thus, as $\mathbb{E} \to +0$, from Eq. (20), one gets:

$$\langle\mathbb{E}_k^{a-\frac{1}{2}}\rangle_{KIM} \to 0, \tag{23}$$

being in good agreement with our result obtained in Eq. (A3) of the Appendix A.

In summary, from Eqs. (22, 23) and for $\underline{\mathbb{E} \geq 0}$, the expression of $\langle\mathbb{E}_k^{a-\frac{1}{2}}\rangle_{KIM}$ can be approximated by:

$$\langle\mathbb{E}_k^{a-\frac{1}{2}}\rangle_{KIM} \cong \mathbb{E}^{a-\frac{1}{2}}. \tag{24}$$

$\mathbb{E} \leq 0$-case

Here, from Eqs. (19, 21), Eq. (20) can be rewritten as

$$\langle\mathbb{E}_k^{a-\frac{1}{2}}\rangle_{KIM} = \frac{\exp(-x^2/4)\times W_n^{\frac{2a-1}{4}}}{\sqrt{2\pi}} \times \Gamma(a+\tfrac{1}{2}) \times D_{-a-\frac{1}{2}}(x),$$

$$= \frac{\exp(-x^2/4)\times \eta_n^{a-\frac{1}{2}}}{\sqrt{2\pi}} \times \exp\left(-\frac{\mathcal{H}_n R_{sn}\times(2a-1)}{8\times\sqrt{|\nu_n|}}\right) \times \Gamma(a+\tfrac{1}{2}) \times D_{-a-\frac{1}{2}}(x). \tag{25}$$

As $\mathbb{E} \to -0$, from Eq. (21), one has: $\nu_n \to +0$ and $x \to +\infty$. Thus, one obtains, for any $a \geq 1$, [15]

$D_{-a-\frac{1}{2}}(x\to\infty)\simeq\beta(a)\times\exp\left[-(\sqrt{a}+\frac{1}{16a^{\frac{3}{2}}})\,x-\frac{x^2}{16a}-\frac{x^3}{24\sqrt{a}}\right]\to 0$, $\beta(a)=\frac{\sqrt{\pi}}{2^{\frac{2a+1}{4}}\Gamma(\frac{a}{2}+\frac{3}{4})]}$, noting that

$$\beta(1)=\frac{\sqrt{\pi}}{2^{\frac{3}{4}}\times\Gamma(5/4)}\text{ and }\beta(5/2)=\frac{\sqrt{\pi}}{2^{3/2}}.$$

Then, putting $f(a)\equiv\frac{\eta_n^{a-\frac{1}{2}}}{\sqrt{2\pi}}\times\Gamma(a+\frac{1}{2})\times\beta(a)$, Eq. (25) yields

$$H_n(\nu_n\to 0,r_d,a)=\frac{\langle\mathbb{E}_k^{a-\frac{1}{2}}\rangle_{KIM}}{f(a)}=\exp\left[-\frac{\mathcal{H}_n R_{sn}\times(2a-1)}{8\times\sqrt{|\nu_n|}}-\left(\sqrt{a}+\frac{1}{16a^{\frac{3}{2}}}\right)x-\left(\frac{1}{4}+\frac{1}{16a}\right)x^2-\frac{x^3}{24\sqrt{a}}\right]\to 0, \quad (26)$$

which is in good accordance with that given in Eq. (A3) of the Appendix A. In particular, as $\nu_n\to 0$, the first term of $\ln H_n(\nu_n\to 0,r_d,a=1)$ given in Eq. (26), $-\frac{\mathcal{H}_n R_{sn}}{8\times\sqrt{|\nu_n|}}$, can be compared with the third one given in Eq. (A3), $-4Bc^2R_{sn}\times|\nu_n|^{-\frac{1}{2}}$. Moreover, as noted in Eqs. (B.5, B.6) of the Appendix B, when the small time approximation (STA) is used: $\Delta r\simeq 0$ [17, 21, 22, 29, 30], $W_n(\nu_n,N)\simeq\eta_n^2$. Therefore, Eq. (25) now yields [21, 29, 30]:

$$H_{n(STA)}(\nu_n\to 0,r_d,a)=\frac{\langle\mathbb{E}_k^{a-\frac{1}{2}}\rangle_{KIM}}{f(a)}=\exp\left[\left(\sqrt{a}+\frac{1}{16a^{\frac{3}{2}}}\right)\times\frac{\mathbb{E}}{\eta_n}\right],\ \mathbb{E}\le 0,$$

being equal to 1 for $\mathbb{E}=-0$, which is not correct, since we must have: $H_n(\mathbb{E}\to-0,r_d,a)\to 0$, as obtained in Eq. (26), due correctly to the Heisenberg uncertainty relation given in Eq. (B.5): $\Delta r\gg 0$ as $\mathbb{E}\to-0$. Finally, we also remark that, in the full ground-state case and deep-tail approximation, the exponential conduction- band tail, obtained by Sa-yakamit et al. [23], was also equal to a constant at $\mathbb{E}=-0$, being not correct.

Further, from Eq. (21), as $\mathbb{E}\to-\infty$, one has: $\nu_n\to+\infty$ and $x\to\infty$. Thus, one gets [15]:

$D_{-a-\frac{1}{2}}(x\to\infty)\approx x^{-a-\frac{1}{2}}\times e^{-\frac{x^2}{4}}\to 0$. Therefore, Eq. (25) yields

$$K_n(\nu_n\to+\infty,r_d,a)\equiv\frac{\langle\mathbb{E}_k^{a-\frac{1}{2}}\rangle_{KIM}}{f(a)}\simeq\frac{1}{\beta(a)}\times\exp\left(-\frac{(A_n\times\nu_n)^2}{2}\right)\times(A_n\times\nu_n)^{-a-\frac{1}{2}}\to 0, \quad (27)$$

being in perfect agreement with a well-known semi-classical Kane's result [14].

It should be noted that, as $\mathbb{E}\le 0$, the ratios (26) and (27) can be taken in an approximate form as

$$F_n(\nu_n,r_d,a)=K_n(\nu_n,r_d,a)+[H_n(\nu_n,r_d,a)-K_n(\nu_n,r_d,a)]\times\exp[-c_1\times(A_n\nu_n)^{c_2}], \quad (28)$$

so that: $F_n(\nu_n,r_d,a)\to H_n(\nu_n,r_d,a)$ for $0\le\nu_n\le 16$, and $F_n(\nu_n,r_d,a)\to K_n(\nu_n,r_d,a)$ for $\nu_n\ge 16$. For that, in next sections V and VI, the constants c_1 and c_2 may be respectively chosen as: $c_1=10^{-40}$ and $c_2=80$ when $a=1$, being used to the study of reduced density of exponential conduction-band-tail states, and $c_1=20^{-150}$ and $c_2=300$ when $a=5/2$, for the study of reduced optical absorption coefficient and exponential tails of electrical conductivity.

Here, one remarks that, from Eqs. (26-28) and for a given value of a, since, as $\nu_n\to+0$ and $+\infty$, $F_n(\nu_n,r_d,a)\to 0$, the maximum of this function thus exists, occurring at $\nu_n=\nu_{n(M)}$. Hence, in various degenerate d-Si systems, in which $N=5\times10^{20}$ cm^{-3} and T=0 K, for example, using Eq. (28), we can study the behaviors of the function $\ln[F_n(\nu_n,r_d,a)]<0$, for given a, which can take its approximate form determined by: $AF(\nu_n,r_d,\nu_1,\nu_2,z,f)<0$, obtained in small ν_n-intervals: $\nu_1\le\nu_n\le\nu_2$, as

$$AF(\nu_n,r_d,\nu_1,\nu_2,z,f)=e(r_d,\nu_1,\nu_2,z)\times\nu_n^z+f. \quad (29)$$

Here, $e(r_d,\nu_1,\nu_2,z)$ is the slope of this AF-curve, defined by

$$e(r_d,\nu_1,\nu_2,z)\equiv\frac{\ln F_n(\nu_2,r_d,a)-\ln F_n(\nu_1,r_d,a)}{\nu_2^z-\nu_1^z}, \quad (30)$$

which is negative for $\nu_n>\nu_{n(M)}$ and positive for $\nu_n<\nu_{n(M)}$, noting that for $\nu_n>\nu_{n(M)}$ or in particular $\nu_n\to+\infty$, from our above results (27, 28), one has: z=2. So, for $\nu_n>\nu_{n(M)}$ the values of exponent z=1, ½, 1/3 and ¼, and for $\nu_n<\nu_{n(M)}$ those of exponent z=2, 1, for ½, 1/3 and ¼ could be considered in next Sections V-VII. Moreover, as $\nu_n>\nu_{n(M)}$, according to $e(r_d,\nu_1,\nu_2,z=1)<0$, the energy parameter characteristic of $(-|e|\times\nu_n)$-linear exponential tail states of the function $F_n(\nu_n,r_d)$ can be defined by

$$\mathbb{E}_{no}(N,r_d,\nu_1,\nu_2)\equiv\frac{\mathbb{E}_{Fno}(N)}{|e(r_d,\nu_1,\nu_2,z=1)|}, \quad (31)$$

as observed in next Figs. 2, 5, and 8.

It should be noted that the important results (20) obtained for any $\mathbb{E}$-values, (24) for $\mathbb{E}\ge 0$, and (28-31) for $\mathbb{E}\le 0$, can be used to determine the density of states and the optical,

electrical and thermoelectric functions in Sections V-VIII, respectively.

4. Low Temperature Effect, Due to the Fermi-Dirac Distribution Function

The Fermi-Dirac distribution function (FDDF) is given by

$$f(\mathbb{E}) \equiv (1+e^{\gamma})^{-1}, \gamma \equiv (\mathbb{E}-\mathbb{E}_{Fn})/(k_B T),$$

where $\mathbb{E}_{Fn}(N,T)$ is the Fermi energy determined in Eq. (A10) of the Appendix C.

So, the average of $\mathbb{E}^p$, calculated using the FDDF, can be defined as

$$\langle \mathbb{E}^p \rangle_{FDDF} \equiv G_p(\mathbb{E}_{Fn}) \times \mathbb{E}_{Fn}^p \equiv \int_{-\infty}^{\infty} \mathbb{E}^p \times \left(-\frac{\partial f}{\partial \mathbb{E}}\right) d\mathbb{E}, -\frac{\partial f}{\partial \mathbb{E}} = \frac{1}{k_B T} \times \frac{e^{\gamma}}{(1+e^{\gamma})^2}. \quad (32)$$

Further, one remarks that, at 0 K, $-\frac{\partial f}{\partial \mathbb{E}} = \delta(\mathbb{E}-\mathbb{E}_{Fno})$, $\delta(\mathbb{E}-\mathbb{E}_{Fno})$ being the Dirac delta (δ)-function and $\mathbb{E}_{Fno}$ is the Fermi energy at T=0 K defined in Eq. (15). Therefore, $G_p(\mathbb{E}_{Fno}) = 1$.

Then, at low T, by a variable change $\gamma \equiv (\mathbb{E}-\mathbb{E}_F)/(k_B T)$, Eq. (32) yields

$$G_p(\mathbb{E}_{Fn}) \equiv 1 + \mathbb{E}_{Fn}^{-p} \times \int_{-\infty}^{\infty} \frac{e^{\gamma}}{(1+e^{\gamma})^2} \times (k_B T\gamma + \mathbb{E}_{Fn})^p d\gamma = 1 + \sum_{\mu=1,2,...}^{p} C_p^{\beta} \times (k_B T)^{\beta} \times \mathbb{E}_{Fn}^{-\beta} \times I_{\beta},$$

where $C_p^{\beta} \equiv p(p-1)...(p-\beta+1)/\beta!$ and the integral I_{β} is given by

$$I_{\beta} = \int_{-\infty}^{\infty} \frac{\gamma^{\beta} \times e^{\gamma}}{(1+e^{\gamma})^2} d\gamma = \int_{-\infty}^{\infty} \frac{\gamma^{\beta}}{\left(e^{\gamma/2}+e^{-\gamma/2}\right)^2} d\gamma,$$

vanishing for old values of β. Then, for even values of $\beta = 2n$, with n=1, 2, …, one obtains

$$I_{2n} = 2\int_0^{\infty} \frac{\gamma^{2n} \times e^{\gamma}}{(1+e^{\gamma})^2} d\gamma. \quad (33)$$

Now, using an identity [15]: $(1+e^{\gamma})^{-2} \equiv \sum_{s=1}^{\infty} (-1)^{s+1} s \times e^{\gamma(s-1)}$, a variable change: $s\gamma = -t$, the Gamma function: $\int_0^{\infty} t^{2n} e^{-t} dt \equiv \Gamma(2n+1) = (2n)!$, and also the definition of the Riemann's zeta function [15]: $\zeta(2n) \equiv 2^{2n-1}\pi^{2n}|B_{2n}|/(2n)!$, B_{2n} being the Bernoulli numbers, one finally gets: $I_{2n} = (2^{2n}-2) \times \pi^{2n} \times |B_{2n}|$. So, from Eq. (32), we get in the degenerate case the following ratio:

$$G_p(\mathbb{E}_{Fn}) \equiv \frac{\langle \mathbb{E}^p \rangle_{FDDF}}{\mathbb{E}_{Fn}^p} = 1 + \sum_{n=1}^{p} \frac{p(p-1)...(p-2n+1)}{(2n)!} \times (2^{2n}-2) \times |B_{2n}| \times y^{2n} \equiv G_p(y), y = \frac{\pi k_B T}{\mathbb{E}_{Fn}} \simeq \frac{\pi k_B T}{\mathbb{E}_{Fno}}. \quad (34)$$

It should be noted that our previous expression for $G_p(x)$ [58] can now be corrected, replacing β by 2n and the Bernoulli numbers $B_{\beta/2}$ by $|B_{2n}|$. Further, Jaffe [49] proposed the following result:

$$G_{p(Jaffe)}(\mathbb{E}_{Fn}, T) = 1 + \mathbb{E}_{Fn}^{-p} \times \sum_{n=1}^{p} (-1)^{2n+1} \times c_{2n} \times (k_B T)^{2n} \times \left(\frac{d^{2n}}{d\mathbb{E}^{2n}} \mathbb{E}^p\right)_{\mathbb{E}=\mathbb{E}_{Fn}}, \quad (35)$$

where $c_{2n} = \frac{(2-2^{2n}) \times \pi^{2n} \times |B_{2n}|}{(2n)!}$. Now, using an identity:

$$\left(\frac{d^{2n}}{d\mathbb{E}^{2n}} \mathbb{E}^p\right)_{\mathbb{E}=\mathbb{E}_{Fn}} \equiv p(p-1)...(p-2n+1) \times \mathbb{E}_{Fn}^{p-2n},$$

Eq. (35) is found to be identical to our above result (34), which is a more practical result. Then, some usual results of $G_p(y)$ are given in Table 3.

Table 3. *The values of absolute Bernoulli numbers $|B_{2n}|$ [15], and some expressions for $G_p(y)$, obtained from Eq. (34) at low T and for $p \geq 3/2$. Here, $y = \frac{\pi k_B T}{\mathbb{E}_{Fn}} \simeq \frac{\pi k_B T}{\mathbb{E}_{Fno}}$.*

2n	2	4	6	8	10	12
$\lvert B_{2n}\rvert$	1/6	$\lvert -1/30\rvert$	1/42	$\lvert -1/30\rvert$	5/66	$\lvert -691/2730\rvert$

$G_{\frac{3}{2}}(y) = 1 + \frac{y^2}{8} + \frac{7y^4}{640}$, $G_2(y) = 1 + \frac{y^2}{3}$, $G_{\frac{5}{2}}(y) = 1 + \frac{5y^2}{8} - \frac{7y^4}{384}$, $G_3(y) = 1 + y^2$, $G_{\frac{7}{2}}(y) = 1 + \frac{35y^2}{24} + \frac{49y^4}{384}$, $G_4(y) = 1 + 2y^2 + \frac{7y^4}{15}$, $G_{\frac{9}{2}}(y) = 1 + \frac{21y^2}{8} + \frac{147y^4}{128}$, …

These functions $G_p(y)$ obtained in Table 3 will be applied to determine the electrical and thermoelectric properties of the degenerate d-Si systems, being given in Sections 7 and 8, respectively.

5. Determination of Critical Donor Density

In degenerate d-Si systems at T=0 K, due to the heavy doping effect (HDE), using Eq. (20) for a=1, $\langle \mathbb{E}_k^{\frac{1}{2}} \rangle_{KIM}$, the density of states $\mathcal{D}(\mathbb{E})$ is given by:

$$\langle \mathcal{D}(\mathbb{E}_k) \rangle_{KIM} \equiv \frac{g_c}{2\pi^2} \left(\frac{2m_n^{HDE}(N)}{\hbar^2} \right)^{\frac{3}{2}} \times \langle \mathbb{E}_k^{\frac{1}{2}} \rangle_{KIM} = \frac{g_c}{2\pi^2} \left(\frac{2m_n^{HDE}(N)}{\hbar^2} \right)^{\frac{3}{2}} \times \frac{\exp\left(-\frac{x^2}{4}\right) \times W_n^{\frac{1}{4}}}{\sqrt{2\pi}} \times \Gamma\left(\frac{3}{2}\right) \times D_{-\frac{3}{2}}(x) = \mathcal{D}(\mathbb{E}), \quad (36)$$

where $m_n^{HDE}(N)$ is the electron effective mass, due to the HDE, determined in Eq. (8), and the variable x is defined in Eq. (21), as

$$x = \frac{-\mathbb{E}}{\sqrt{W_n}} \equiv A_n \times \nu_n \times \exp\left(\frac{\mathcal{H}_n \times R_{sn}}{4 \times \sqrt{|\nu_n|}} \right), A_n \equiv \frac{\mathbb{E}_{Fno}}{\eta_n}, \nu_n(\mathbb{E}, N) \equiv \frac{-\mathbb{E}}{\mathbb{E}_{Fno}}.$$

Here, $\mathbb{E}_{Fno}$ is determined in Eq. (15) for $m^* = m_n^{HDE}(N)$, $m_n^{HDE}(N)$ being the electron effective mass due to the HDE and determined in Eq. (8), and the value of Heisenberg empirical parameter $\mathcal{H}_{n(p)}$ was defined in the Appendix B and proposed here as: $\mathcal{H}_{n(p)}$=5.4370, so that the following determination of the critical density of electrons localized in the exponential conduction-band tail would be accurate. Further, from Eq. (24), one also has

$$\mathcal{D}(\mathbb{E} \geq 0) = \frac{g_c}{2\pi^2} \left(\frac{2m_n^{HDE}(N)}{\hbar^2} \right)^{\frac{3}{2}} \times \sqrt{\mathbb{E}}. \quad (37)$$

Going back to the functions: H_n, K_n and F_n, given respectively in Eqs. (26-28), in which the factor $\frac{\langle \mathbb{E}_k^{\frac{1}{2}} \rangle_{KIM}}{f(a=1)}$ is now replaced by:

$$\frac{\langle \mathbb{E}_k^{\frac{1}{2}} \rangle_{KIM}}{f(a=1)} = \frac{\mathcal{D}(\mathbb{E} \leq 0)}{\mathcal{D}_o} = F_n(\nu_n, r_d, a=1), \mathcal{D}_o = \frac{g_c \times (m_n^{HDE})^{3/2} \times \sqrt{\eta_n}}{2\pi^2 \hbar^3} \times \beta(a=1), \beta(a=1) = \frac{\sqrt{\pi}}{2^{\frac{3}{4}} \times \Gamma(5/4)}, \quad (38)$$

where the reduced density of exponential-tail states: $F_n(\nu_n, r_d, a=1) \equiv F_{n(1)}(\nu_n, r_d)$, for a simplicity of presentation, is determined in Eq. (28). Then, in d-Si systems at 0 K and for $N = 5 \times 10^{20}$ cm^{-3}, our results of the functions $F_{n(1)}(\nu_n, r_d)$ obtained for each r_d-value, are plotted as functions of ν_n in Figure 1.

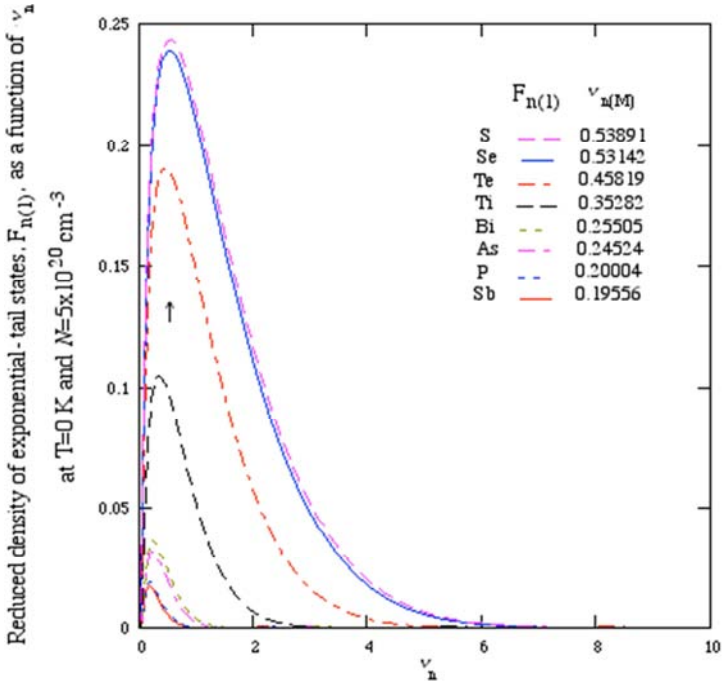

Figure 1. *Our results of $F_{n(1)}$ increase with increasing r_d for a given ν_n, due to the donor-size effect, and present the maxima at $\nu_n = \nu_{n(M)}$ and go to zero as $\nu_n \to 0$ and ∞.*

Figure 1 shows that:

(i) our results of $F_{n(1)}$ increase with increasing r_d for a given ν_n, due to the donor-size effect, and

(ii) present the maxima at $\nu_n = \nu_{n(M)}$ and go to zero as $\nu_n \to 0$ and ∞, being found to be in good agreement with theoretical results obtained by Lifshitz [18], Friedberg and Luttinger [20], our results given in Eq. (A.3) of the Appendix A, and in particular with an asymptotic form for exponential conduction-band tail, obtained for $0 \lesssim \nu_n \lesssim \infty$, by Halperin and Lax [19], using the minimum counting methods.

Further, our numerical results of functions $\ln[F_n(\nu_n, r_d, a = 1)] < 0$, which can take their approximate forms as: $AF(\nu_n, r_d, \nu_1, \nu_2, z, f) = e(r_d, \nu_1, \nu_2, z) \times \nu_n^z + f < 0$, obtained in small ν_n-intervals: $\nu_1 \le \nu_n \le \nu_2$, using Eqs. (29, 30), are tabulated in Table 4.

Table 4. *In the d-Si systems at T=0 K and for $N = 5 \times 10^{20}\ cm^{-3}$, using the reduced density of state, $F_n(\nu_n, r_d, a = 1)$, determined in Eq. (38), the numerical results of $ln[F_n(\nu_n, r_d, a = 1)]$ and its approximate form obtained for a=1: $AF(\nu_n; r_d, \nu_1, \nu_2, z, f) = e(r_d, \nu_1, \nu_2, z) \times \nu_n^z + f$, determined in Eqs. (29, 30) for small ν_n-intervals: $\nu_1 \le \nu_n \le \nu_2$, and also those of absolute relative errors defined by: $|RE| \equiv 1 - \frac{AF(\nu_n, r_d, \nu_1, \nu_2, z, f)}{ln[F_n(\nu_n, r_d, a=1)]}$, are evaluated and tabulated below.*

Donor	**Sb**	**P**	**As**	**Bi**	**Ti**	**Te**	**Se**	**S**
$\nu_{n(M)}$	**0.19556**	**0.20004**	**0.24524**	**0.25505**	**0.35282**	**0.45819**	**0.53142**	**0.53891**
For $1.20 \le \nu_n \le 1.25$, $AF = (e \times \nu_n + f)$ is accurate to within 2.2×10^{-4}, where								
-e	10.312	9.433	5.642	5.037	1.846	0.854	0.567	0.546
f	1.387	1.016	-0.374	-0.552	-1.118	-1.056	-0.994	-0.988
|RE|	8.1×10^{-5}	9.9×10^{-5}	6.3×10^{-5}	1.2×10^{-4}	2.2×10^{-4}	1.0×10^{-4}	5.4×10^{-5}	6.3×10^{-5}
For $1.10 \le \nu_n \le 1.20$, $AF = (e \times \nu_n^{1/2} + f)$ is accurate to within 6.6×10^{-4}, where								
-e	21.192	19.400	11.654	10.413	3.825	1.759	1.159	1.114
f	12.233	10.953	5.624	4.813	0.857	-0.154	-0.405	-0.423
|RE|	6.6×10^{-4}	5.8×10^{-4}	5.6×10^{-4}	5.5×10^{-4}	3.6×10^{-4}	4.4×10^{-4}	5.3×10^{-4}	4.7×10^{-4}
For $1.07 \le \nu_n \le 1.09$, $AF = (e \times \nu_n^{1/3} + f)$ is accurate to within 3.1×10^{-4}, where								
-e	29.952	27.445	16.549	14.795	5.442	2.484	1.619	1.555
f	20.921	18.933	10.483	9.162	2.462	0.566	0.510	0.014
|RE|	3.8×10^{-5}	7.9×10^{-5}	3.5×10^{-5}	3.2×10^{-5}	1.7×10^{-4}	3.1×10^{-4}	4.9×10^{-5}	2.7×10^{-5}
For $\nu_{n(M)} < 1.00 \le \nu_n \le 1.05$, $AF = (e \times \nu_n^{1/4} + f)$ is accurate to within 3.2×10^{-4}, where								
-e	37.375	34.267	20.721	18.533	6.815	3.084	1.989	1.908
f	28.308	25.723	14.636	12.883	3.829	1.162	0.419	0.365
|RE|	2.6×10^{-4}	2.3×10^{-4}	2.1×10^{-4}	2.3×10^{-4}	2.3×10^{-4}	2.2×10^{-4}	3.2×10^{-4}	2.7×10^{-4}
For $0.090 \le \nu_n \le 0.095 < \nu_{n(M)}$, $AF = (e \times \nu_n^{1/4} + f)$ is accurate to within 3.5×10^{-4}, where								
e	16.603	17.281	19.424	19.467	15.283	11.155	9.666	9.554
f	-13.968	-14.322	-15.240	-15.172	-11.807	-8.815	-7.728	-7.646
|RE|	2.9×10^{-4}	2.7×10^{-4}	3.0×10^{-4}	2.4×10^{-4}	3.5×10^{-4}	2.2×10^{-4}	3.3×10^{-4}	1.3×10^{-4}
For $0.088 \le \nu_n \le 0.090$, $AF = (e \times \nu_n^{1/3} + f)$ is accurate to within 1.9×10^{-4}, where								
e	16.618	17.279	19.346	19.376	15.067	10.876	9.372	9.258
f	-12.322	-12.601	-13.271	-13.193	-10.188	-7.579	-6.634	-6.562
|RE|	9.5×10^{-5}	1.1×10^{-4}	1.0×10^{-4}	1.5×10^{-4}	1.5×10^{-4}	1.6×10^{-4}	1.9×10^{-4}	1.1×10^{-4}
For $0.080 \le \nu_n \le 0.083$, $AF = (e \times \nu_n^{1/2} + f)$ is accurate to within 2.8×10^{-4}, where								
e	20.696	21.486	23.925	23.934	18.238	12.825	10.903	10.758
f	-11.049	-11.269	-11.741	-11.652	-8.881	-6.537	-5.692	-5.628
|RE|	1.5×10^{-4}	2.2×10^{-4}	2.2×10^{-4}	1.9×10^{-4}	1.4×10^{-4}	2.7×10^{-4}	2.8×10^{-4}	1.4×10^{-4}
For $0.061 \le \nu_n \le 0.064$, $AF = (e \times \nu_n + f)$ is accurate to within 6.4×10^{-4}, where								
e	81.678	84.899	95.187	95.220	69.115	44.628	36.206	35.580
f	-11.286	-11.520	-12.064	-11.976	-8.887	-6.265	-5.341	-5.271
|RE|	4.8×10^{-4}	6.4×10^{-4}	5.2×10^{-4}	5.4×10^{-4}	4.4×10^{-4}	4.3×10^{-4}	3.3×10^{-4}	2.9×10^{-4}
For $0.054 \le \nu_n \le 0.056$, $AF = (e \times \nu_n^2 + f)$ is accurate to within 4.9×10^{-4}, where								
e	1119.900	1167.630	1327.600	1330.280	948.984	585.600	462.692	453.624
f	-10.322	-10.531	-11.015	-10.934	-8.074	-5.648	-4.799	-4.735
|RE|	3.4×10^{-4}	3.8×10^{-4}	4.7×10^{-4}	4.9×10^{-4}	4.6×10^{-4}	3.7×10^{-4}	2.5×10^{-4}	2.5×10^{-4}

The underlined $|RE|$-value is the maximal one for each donor-Si system.

Table 4 suggests that: (i) our results of $AF(\nu_n, r_d, \nu_1, \nu_2, z, f)$ given for (z=1)-exponent agree with the Urbach law obtained from linear exponential conduction-band-tail behaviors by some workers [21, 29, 30, 37], (ii) ours for (z=1/2)-exponent and $\nu_n > \nu_{n(M)}$ agree with other theoretical results [19, 37], and finally (iii) ours for (z=1/3, 1/4)-exponents when $\nu_n > \nu_{n(M)}$, and for (z=1/4, 1/3, ½, 1, 2)-exponents when $\nu_n < \nu_{n(M)}$ may thus be new.

Finally, our numerical results of energy parameter, $\mathbb{E}_{no}(N; r_d, a = 1)$, obtained in the small interval: $1.2 \le \nu_n \le 1.25$, using Eq. (31), are plotted as functions of N in Figures 2a and 2b, indicating that, for a given N, $\mathbb{E}_{no}$ increases with increasing r_d-values, due to the donor-size effect.

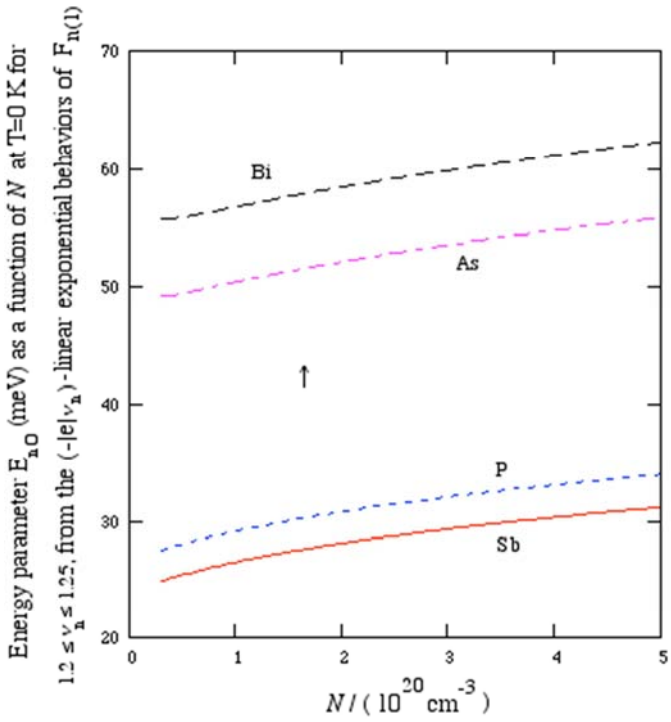

FIG. 2a

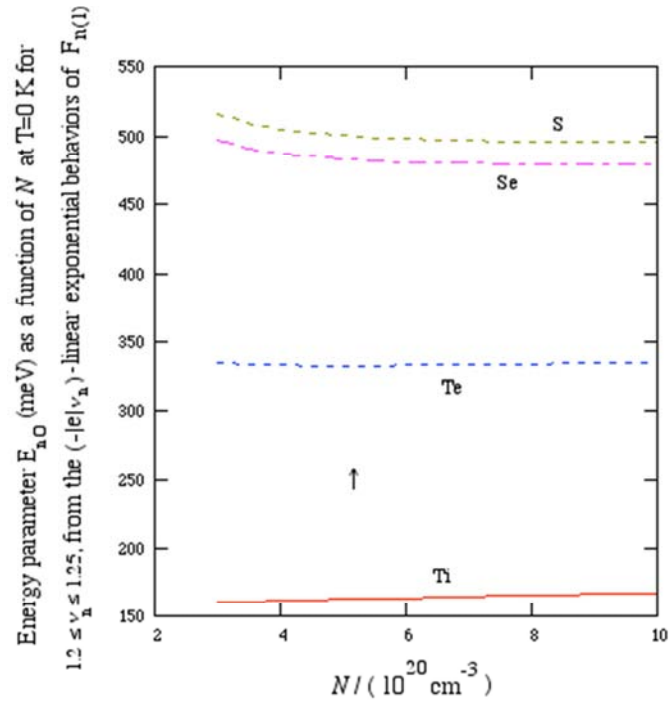

FIG. 2b

Figures 2. *Our results of energy parameter, $\mathbb{E}_{no}(N; r_d, a = 1)$, are plotted as functions of N, indicating that, for a given N, $\mathbb{E}_{no}$ increases with increasing r_d-values, due to the donor-size effect.*

Now, for $\mathbb{E} \le 0$, using Eqs. (27, 28) for the functions K_n and F_n as a=1, the density of electrons localized in the exponential band tail (EBT) is given by

$$N_d^{EBT}(N, r_d) = \int_{-\infty}^{0} \mathcal{D}(\mathbb{E} \le 0)\, d\mathbb{E}, \tag{39}$$

where $\mathcal{D}(\mathbb{E} \le 0)$ is determined in Eq. (38).

Then, by a variable change: $\nu_n \equiv \frac{-\mathbb{E}}{\mathbb{E}_{Fno}}$, Eq. (39) yields

$$N_{d,\mathscr{b}}^{EBT}(N, r_d) = \frac{g_c \times (m_n^{HDE})^{3/2} \sqrt{\eta_n} \times \mathbb{E}_{Fno}}{2\pi^2 \hbar^3} \times \mathscr{b} \times \left\{ \int_0^{16} \beta(a=1) \times F_n(\nu_n, r_d, a=1)\, d\nu_n + I_n \right\}, \quad (40)$$

where

$$I_n \equiv \int_{16}^{\infty} \beta(a=1) \times K_n(\nu_n, r_d, a=1)\, d\nu_n = \int_{16}^{\infty} e^{\frac{-(A_n \nu_n)^2}{2}} \times (A_n \nu_n)^{-3/2}\, d\nu_n.$$

Here, $\beta(a=1) = \frac{\sqrt{\pi}}{2^{\frac{3}{4}} \times \Gamma(5/4)}$ and $\mathscr{b}$ is normally equal to 1, but it can be an empirical parameter, being chosen as: $\mathscr{b} = \mathscr{b}_o = 1.0028637416$ such that the obtained values of N_n^{EBT} would be accurate.

Then, by another variable change: $t = \left[A_n \nu_n / \sqrt{2}\right]^2$, the integral I_n yields [15]

$$I_n = \frac{1}{2^{5/4} A_n} \times \int_{y_n}^{\infty} t^{b-1} e^{-t} dt \equiv \frac{\Gamma(b, y_n)}{2^{5/4} \times A_n},$$

where $b = -1/4$, $y_n = \left[16 A_n / \sqrt{2}\right]^2$, with A_n being defined in Eq. (38), and $\Gamma(b, y_n)$ is the incomplete Gamma function, defined by [15]

$$\Gamma(b, y_n) \backsimeq y_n^{b-1} \times e^{-y_n} \left[1 + \sum_{j=1}^{16} \frac{(b-1)(b-2)\ldots(b-j)}{y_n^j}\right].$$

Finally, Eq. (40) now yields

$$N_{d,\mathscr{b}}^{EBT}(N, r_d) = \frac{g_c \times (m_n^{HDE})^{3/2} \sqrt{\eta_n} \times \mathbb{E}_{Fno}}{2\pi^2 \hbar^3} \times \mathscr{b} \times \left\{ \int_0^{16} \beta(a=1) \times F_n(\nu_n, r_d, a=1)\, d\nu_n + \frac{\Gamma(b, y_n)}{2^{5/4} \times A_n} \right\}, \quad (41)$$

being the density of electrons localized in the exponential conduction-band tail.

Hence, in the degenerate d-Si system, replacing N, given in the parabolic conduction band of an effective electron gas, by the effective density of free electrons defined here by: $N^* = N - N_{d,\mathscr{b}}^{EBT} \geq 0$. So, in this system, the Fermi energy given in Eq. (15) is now rewritten as

$$\mathbb{E}_{Fno}(N^*) \equiv \frac{\hbar^2 \times k_{Fn}^2(N^*)}{2 \times m_n^{HDE}(N^*)},\ N \geq N_{d,\mathscr{b}}^{EBT}, \quad (42)$$

where the Fermi wave number k_{Fn} and m_n^{HDE} are respectively determined in Eqs. (2, 8). One notes here that $\mathbb{E}_{Fno}(N^*)$ vanishes at $N^* = 0$, or at the critical donor density defined by: $N = N_{c(d),\mathscr{b}}^{EBT} \equiv N_{d,\mathscr{b}}^{EBT}(N = N_{c(d),\mathscr{b}}^{EBT}, r_d)$, at which the metal-insulator transition thus occurs. Then, the numerical results of $N_{c(d),\mathscr{b}}^{EBT}$, for $\mathscr{b} = 1$ and $\mathscr{b}_o = 1.0028637416$, and their absolute relative errors $|RE|$, calculated using the $N_{c(d)}$-data given in Table I, are obtained and also reported in this Table 1, indicating that those of $N_{c(d),\mathscr{b}_o}^{EBT}$ and $N_{c(d),1}^{EBT}$ are obtained respectively with accuracies of the orders of 1.1×10^{-4} and 3×10^{-3}. Hence, these results of $N_{c(d),\mathscr{b}_o}^{EBT}$ thus confirm our above choice of Heisenberg parameter value: $\mathcal{H}_n$=5.4370, as that proposed in Eq. (19) and also in the Appendix B. Furthermore, our numerical calculation indicates that, in all the d-Si systems for $N \geq 1.15 \times N_{c(d)}$, if defining the absolute relative deviations between $N - N_{c(d),\mathscr{b}_o}^{EBT}$ and N- $N_{c(d)}$ by: $|RD| \equiv \left|1 - \frac{N_{c(d),\mathscr{b}_o}^{EBT}}{N - N_{c(d)}}\right|$, the maximal $|RD|$ -values, which occur at $N = 1.15 \times N_{c(d)}$, are approximately equal to 3.2%. So, N^* given in the parabolic conduction band of the degenerate d-Si systems can be approximated by [22]

$$N^* \equiv N - N_{c(d),\mathscr{b}_o}^{EBT} \simeq N - N_{c(d)}. \quad (43)$$

Here, this notion of effective density of free electrons N^* defined by Eq. (43) should be equivalent to that of $(N_d - N_a)$ given in the n-type compensated Si, in which N_d is the total density of donors (or majority electrons) and N_a is the total density of acceptors (or minority holes), assuming that all the impurities are ionized [22]. Finally, in degenerate d-Si systems, in which $N > N_{c(d)}$ and $T \leq 77$ K or $T \ll T_D$, T_D being the degeneracy temperature defined in Eq. (15), this result (43) will be used in all the following Sections.

6. Optical Properties

The problem of exponential optical absorption-coefficient tails has by now a rather long history. We will limit our study here to the degenerate d-Si systems, although the band structure of random alloys and amorphous materials is a problem with many common features [41].

Optical properties of any medium can be described by the complex refraction index $\mathbb{N}$ and the complex dielectric function ε, defined by: $\mathbb{N} \equiv n - i\kappa$ and $\varepsilon \equiv \varepsilon_1 - i\varepsilon_2$, where $i^2 = -1$ and $\varepsilon \equiv \mathbb{N}^2$, and by the optical absorption coefficient α, which is related to the imaginary part of ε: ε_2, the refraction index n, the extinction coefficient κ, and the conductivity σ_O, due to the electro-optical effect, as [29-48]

$$\alpha(E) \equiv \frac{\hbar q^2 \times |v(E)|^2}{n(E) \times \varepsilon_o c E} \times J(E) = \frac{E \times \varepsilon_2(E)}{\hbar c n(E)} = \frac{2E \times \kappa(E)}{\hbar c} = \frac{4\pi \times \sigma_O(E)}{c n(E) \times \varepsilon_o}. \quad (44)$$

One remarks that the real part of ε is defined by

$$\varepsilon_1(E) \equiv n(E)^2 - \kappa(E)^2, \quad (45)$$

and the normal-incidence reflectance R(E), by

$$R(E) = \frac{[n(E)-1]^2+\kappa(E)^2}{[n(E)+1]^2+\kappa(E)^2}, \quad (46)$$

which are the optical dispersion relations since in general the values of those optical functions are expressed as functions of the multi-photon energy [46], $E \equiv \hbar\omega, 2\hbar\omega$, $3\ \hbar\omega$, $4\hbar\omega$,…. In the present work, we only focus our attention to the case of photon energy $E \equiv \hbar\omega$. Here, *-q, ħ,* $|v(E)|$, *ω,* ε_o, *c* and $J(E)$ respectively represent the electron charge, Dirac's constant, matrix elements of the velocity operator between valence-and-conduction bands in n-type semiconductors, photon frequency, permittivity of free space, velocity of light, and joint density of states (JDOS). One remarks here that: (i) if some optical functions are known such as: (J, n, $|v|^2$), (n, κ), or (ε_1, ε_2), then, all other ones are determined, and (ii) in n-type semiconductors, all the optical functions will be expressed in terms of the total energy of the electron, defined by:

$$\mathbb{E} \equiv E - \mathbb{E}_{gn}, \quad (47)$$

where the band gap given in the degenerate d-Si systems, $\mathbb{E}_{gn}$, can be equal to: $\mathbb{E}_{gi}$, $\mathbb{E}_{gn1}$ and $\mathbb{E}_{gn2}$, defined in Eqs. (3, 9, 10), respectively.

Now, we determine the accurate expressions for the optical functions obtained in band-to-band transitions at $E \geq \mathbb{E}_{gn}$, and for the exponential optical absorption-coefficient tails and also their behaviors at $E \leq \mathbb{E}_{gn}$, due to the effects of temperature, donor size and heavy doping, being also compared with corresponding experimental and theoretical results.

6.1. Optical Functions Obtained in Band-to-Band Transitions at $E \geq \mathbb{E}_{gn}$ or $\mathbb{E} \geq 0$

First of all, one remarks from Eq. (37) that if replacing the density-of-states effective mass, $g_c^{2/3} \times m_n^{HDE}$, by the reduced effective mass $m_r = 0.171 \times m_o$, defined in Eq. (1), the density of state $\mathcal{D}(\mathbb{E} \geq 0)$ becomes the joint density of states, given in Eq. (44), as

$$J(E) = \frac{1}{2\pi^2} \times \left(\frac{2m_r}{\hbar^2}\right)^{3/2} \times (\mathbb{E} \equiv E - \mathbb{E}_{gn})^{(1/2)}.$$

Then, we use a transformation, replacing $(\mathbb{E})^{1/2}$ by: $\frac{1}{\mathbb{E}_{Fno}^{a-1}} \times (\mathbb{E})^{(1/2)+(a-1)=\mathbb{s}=a-\frac{1}{2}}$. So, J(E) yields for $a \geq 1$ as

$$J(E,a) = \frac{1}{2\pi^2} \times \left(\frac{2m_r}{\hbar^2}\right)^{3/2} \times \frac{1}{\mathbb{E}_{Fno}^{a-1}} \times (E - \mathbb{E}_{gn})^{\mathbb{s}=a-\frac{1}{2}},$$

and from Eq. (44), one gets

$$\alpha(E \geq \mathbb{E}_{gn}) \equiv \frac{\hbar q^2 \times |v(E)|^2}{n(E) \times \varepsilon_o c E} \times \frac{1}{2\pi^2} \times \left(\frac{2m_r}{\hbar^2}\right)^{3/2} \times \frac{1}{\mathbb{E}_{Fno}^{a-1}} \times (E - \mathbb{E}_{gn})^{\mathbb{s}=a-\frac{1}{2}}. \quad (48)$$

Further, for any E or $\mathbb{E}$, using Eq. (20), Eq. (48) becomes

$$\alpha(\mathbb{E},a) \equiv \frac{q^2 \times |v(E)|^2}{n(E) \times \varepsilon_o c E} \times \frac{m_r^{3/2}}{\pi^{5/2} \times \hbar^2} \times \frac{\exp(-x^2/4) \times W_n^{\frac{2a-1}{4}}}{\mathbb{E}_{Fno}^{a-1}} \times \Gamma\left(a+\frac{1}{2}\right) \times D_{-a-\frac{1}{2}}(x), \quad (49)$$

where x is defined in Eq. (21), as $x = \frac{-\mathbb{E}}{\sqrt{W_n}} \equiv A_n \times \nu_n \times \exp\left(\frac{\mathcal{H}_n \times R_{sn}}{4 \times \sqrt{|\nu_n|}}\right)$, $A_n \equiv \frac{\mathbb{E}_{Fno}}{\eta_n}$, $\nu_n \equiv \frac{-\mathbb{E}}{\mathbb{E}_{Fno}}$. Here, the Fermi energy $\mathbb{E}_{Fno}$ is determined in Eq. (15), in which $m^* = m_r = 0.171 \times m_o$, noting that for $E \geq \mathbb{E}_{gn}$ or $\mathbb{E} \geq 0$ and from Eq. (22), the result (49) is reduced to Eq. (48). Here, the values of a=1, 2, 5/2, 7/2 and 9/2 correspond to the allowed-direct [29-31]: $\mathbb{s} = \frac{1}{2}$, forbidden-direct [31]: $\mathbb{s} = \frac{3}{2}$, allowed-indirect [31, 46, 47]: $\mathbb{s} = 2$, forbidden-indirect [46, 47]: $\mathbb{s} = 3$, and forbidden-forbidden-indirect transitions [46, 47]: $\mathbb{s} = 4$, respectively.

Then, one also remarks that:

(i) when a=1, according to allowed direct transitions for n-type (GaAs, GaSb, InP, InAs and InSb)-semiconductors [31], $\alpha(E \geq \mathbb{E}_{gn}, a = 1)$, being thus expressed in terms of $(E - \mathbb{E}_{gn})^{1/2}$, is identical to those obtained by Lukes et Somaratna [29], and Van Cong [30], and

(ii) when a=5/2, according to allowed indirect transitions for n-type (Si, Ge and GaP)-semiconductors [31], $\alpha(E \geq \mathbb{E}_{gn}, a = 5/2)$ is now expressed in terms of $(E - \mathbb{E}_{gn})^2$. In 1984, Forouhi- Bloomer (FB) [40] proposed in his FB-method (FB-M) a familiar four-term expression for extinction coefficient, $\kappa(E, 5/2)$, expressed in terms of $(E - \mathbb{E}_{gn})^2$ for both direct-and-indirect band-gap semiconductors, being thus correct only in indirect band-gap ones. Further, their result is not correct when $E \to \infty$ since one must have: $\kappa(E \to \infty) \to 0$ [36, 41]. Furthermore, in the d-Si systems, from Eqs. (44, 48) one can determine the extinction coefficient κ, obtained for a=5/2, as

$$\kappa(E \geq \mathbb{E}_{gn}) \equiv \frac{q^2 \times {m_r}^{3/2}}{\sqrt{2} \times \pi^2 \times \hbar \times n(E) \times \varepsilon_o \times \mathbb{E}_{Fno}^{3/2}} \times |v(E)|^2 \times \frac{(E-\mathbb{E}_{gn})^2}{E^2}. \quad (50)$$

We now propose an improved FB-M (IFB-M).

First, if putting $f(E) \equiv \sum_{i=1}^{4} \frac{A_{i(FB)} \times E^2}{E^2 - B_{i(FB)} E + C_{i(FB)}}$, where the values of empirical parameters: $A_{i(FB)}$, $B_{i(FB)}$ and $C_{i(FB)}$, are given in the FB-M for the Si [40], and simply replacing the band-gap energy $\mathbb{E}_g = 1.06$ eV [40] by $\mathbb{E}_{gn}$, which can be equal to: $\mathbb{E}_{gi}$, $\mathbb{E}_{gn1}$ and $\mathbb{E}_{gn2}$, which are determined respectively in Eqs. (3, 10, 11), we can now propose, as that done by O'Leary et al. for very large values of E, [39]

$$\kappa_{IFB-M}(E \geq \mathbb{E}_{gn}) = f(E) \times \frac{(E-\mathbb{E}_{gn})^2}{E^2} \times \left(\frac{6\ eV}{E}\right)^3, \text{ for } E \geq 6\ eV,$$

$$= f(E) \times \frac{(E-\mathbb{E}_{gn})^2}{E^2}, \text{ for } \mathbb{E}_{gn} \leq E \leq 6\ eV, \quad (51)$$

so that $\kappa_{IFB-M}(E \to \infty)$ goes to 0 as E^{-3}, in good accordance with both experimental [36] and theoretical [41] results.

Secondly, by putting

$$\Delta n(E, A_{i(FB)}, B_{i(FB)}, C_{i(FB)}, \mathbb{E}_{gn}) \equiv \sum_{i=1}^{4} \frac{B_{oi}E+C_{oi}}{E^2-B_{i(FB)}E+C_{i(FB)}} \equiv \Delta n,$$

for a simplicity of presentation, where the empirical parameters, $B_{oi}(A_{i(FB)}, B_{i(FB)}, C_{i(FB)}, \mathbb{E}_{gn})$ and $C_{oi}(A_{i(FB)}, B_{i(FB)}, C_{i(FB)}, \mathbb{E}_{gn})$, are determined respectively in the FB-M [40], in which we now replace $\mathbb{E}_g = 1.06$ eV by $\mathbb{E}_{gn}$ for our IFB-M, we can further propose

$$n_{IFB-M}(E) = n_\infty + n_o \times \Delta n, \text{ for } E \geq 6\ eV,\ n_\infty \equiv \sqrt{\varepsilon_n}$$

$$= 1.93 + \Delta n, \text{ for } \mathbb{E}_{gn} \leq E \leq 6\ eV,$$

$$= 1.93 + \Delta n(\mathbb{E}_{gn}, A_{i(FB)}, B_{i(FB)}, C_{i(FB)}, \mathbb{E}_{gn}), \text{ for } E \leq \mathbb{E}_{gn}, \quad (52)$$

so that $n_{IFB-M}(E \to \infty) \to \sqrt{\varepsilon_n}$, where the values of ε_n are given in Table I, giving a correct asymptotic behavior of $n_{IFB-M}(E)$. Here, n_o is the factor to be determined so that the function $n_{IFB-M}(E)$ for $E \geq 6$ eV is continuous at $E = 6$ eV, depending on T, r_d, and N.

For example, in intrinsic d-Si systems at 298 K, in which $\mathbb{E}_{gn} = \mathbb{E}_{gi}(T = 298\ K, r_d) = 1.125$ eV is determined in Eq. (3), the values of $n_o(r_d)$ are evaluated and tabulated in Table 5.

Table 5. *In intrinsic donor-Si systems at 298 K, the numerical results of Factor $n_o(r_d)$, being due to the donor-size effect and expressed as functions of donor-radius r_d, are determined so that the function $n_{IFB-M}(E)$ given in Eq. (52) for $E \geq 6$ eV is continuous at $E = 6$ eV.*

Donor	Sb	P	As	Bi	Ti	Te	Se	S
$n_o(r_d)$	2.571289	2.482479	2.032121	1.944450	1.290620	0.805033	0.430750	0.384780

As noted in Eqs. (44-46), if from Eqs. (51, 52) the values of $\kappa_{IFB-M}(E)$ and $n_{IFB-M}(E)$ are evaluated, all other optical functions can thus be determined. So, at 298 K and $1.5 \leq E(eV) \leq 6$, in the intrinsic P-Si systems, in which $\mathbb{E}_{gn} = \mathbb{E}_{gi}(T = 298\ K, r_d) = 1.125$ eV is evaluated using Eq. (3), our results of all the optical functions and the corresponding ones obtained from the FB-M, and the absolute errors of those, calculated using the optical-function data obtained by Aspnes and Studna [33], are tabulated in the Table 6.

Table 6. *In intrinsic P-Si systems at 298 K and for $1.5 \leq E(eV) \leq 6$, our numerical results of all the optical functions (OF) are calculated, using Eqs. (44-46, 51, 52) obtained in our IFB-M, and using the OF-data obtained by Aspnes and Studna [33], their absolute maximal relative errors ($|MREs|$) determined at the photon energy E (eV) are also evaluated and tabulated in this Table, in which the corresponding $|MREs|$ obtained in FB-M are also included.*

MRE	E (eV)	ε_1-|MRE|	ε_2-|MRE|	n-|MRE|	κ-|MRE|	R-|MRE|	α-|MRE|
FB-M	1.5						
($n_\infty = 1.95, E_g = 1.06$ eV)	2.2		0.57		0.58		0.58
	4.2	0.66					
	5.0			0.06			
Our IFB-M	1.5		0.40			0.07	
($n_\infty = \sqrt{11.4}, E_{gi} = 1.125$ eV)	2.6				0.41		0.40
	4.3	0.30					
	5.0			0.08			

The underlined $|MRE|$-value is the maximal one for each optical function.

Table 6. In intrinsic P-Si systems at 298 K and for $1.5 \leq E(eV) \leq 6$, our numerical results of all the optical functions (OF) are calculated, using Eqs. (44-46, 51, 52) obtained in our IFB-M, and using the OF-data obtained by Aspnes and Studna [33], their absolute maximal relative errors (|MREs|) determined at the photon energy E (eV) are also evaluated and tabulated in this Table, in which the corresponding |MREs| obtained in FB-M are also included.

Table 6 indicates that our results given in our IFB-M are found to be more accurate than those obtained in the FB-M. Further, our numerical calculation indicates that, for a given E, since $\kappa_{IFB-M}(E)$ given in Eq. (51) is expressed in terms of $(E - \mathbb{E}_{gn})^2$, if $\mathbb{E}_{gn}$ increases (decreases), then other functions such as: $(E - \mathbb{E}_{gn})^2$, $\kappa_{IFB-M}(E)$, $\varepsilon_{2(IFB-M)}(E)$ and $\varepsilon_{1(IFB-M)}(E)$ decrease (increase), respectively. This useful remark will be used in our IFB-M to explain all the following results.

In the intrinsic P-Si system, $\mathbb{E}_{gn} \equiv \mathbb{E}_{gi}(T, r_P)$, calculated from Eq. (3), decreases with increasing T. So, for a given E, our results of $[E - \mathbb{E}_{gi}(T, r_P)]^2$ and $\varepsilon_{1(2)(IFB-M)}(E)$, obtained in absolute values, increase with increasing T, in good

accordance with experimental results [32, 38, 44, 48], as observed in the following Figure 3a.

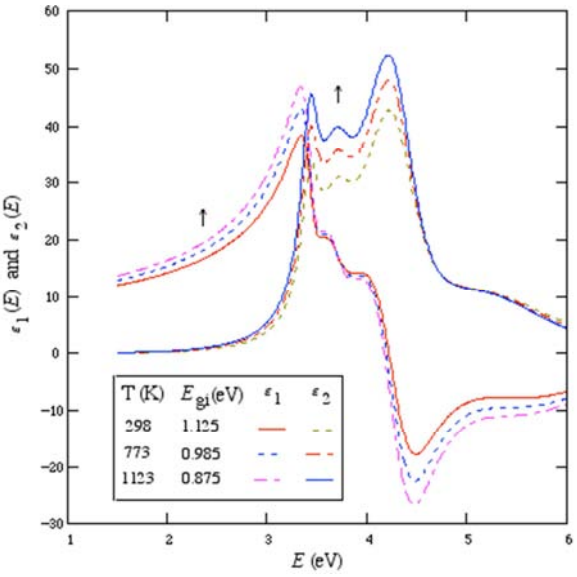

Figure 3a. *In the intrinsic P-Si system, our results of* $\varepsilon_{1(2)(IFB-M)}(E)$*, obtained in absolute values, increase with increasing* T*.*

In intrinsic donor-Si systems, $\mathbb{E}_{gn} \equiv \mathbb{E}_{gi}(r_d, T = 298\ K)$, calculated from Eq. (3), increases with increasing r_d, as seen in Table 1. Thus, for a given E, our results of $[E - \mathbb{E}_{gi}(r_d, T = 298\ K)]^2$ and $\varepsilon_{1(2)(IFB-M)}(E)$, in absolute values, decrease with increasing r_d, as obtained in the following Figure 3b, in which we also observe the correct asymptotic results: $\varepsilon_{1(IFB-M)}(E \to \infty) \to \varepsilon_n$, being identical to the values of ε_n given in Table 1, and $\varepsilon_{2(IFB-M)}(E \to \infty) \to 0$.

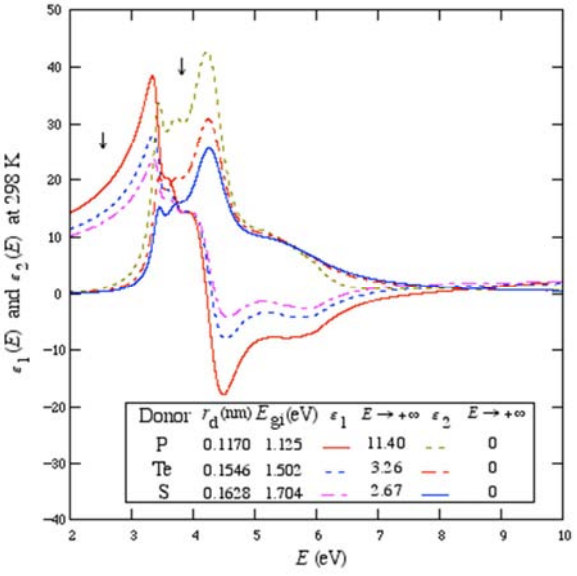

Figure 3b. *In intrinsic donor-Si systems, our results of* $\varepsilon_{1(2)(IFB-M)}(E)$*, in absolute values, decrease with increasing* r_d*.*

In degenerate P-Si systems at T=4.2 K, in which $\mathbb{E}_{gn} \equiv \mathbb{E}_{gn1}(N)$, being the optical band gap determined in Eq. (9), increases with increasing N, due to the heavy-doping effect. So, for a given E, the absolute values of $[E - E_{gn1}(N)]^2$ and $\varepsilon_{1(2)(IFB-M)}(E)$ decrease with increasing N, in good accordance with experiments by Aspnes et al. [34], and Vina and Cardona [35], as seen in the following Figure 3c.

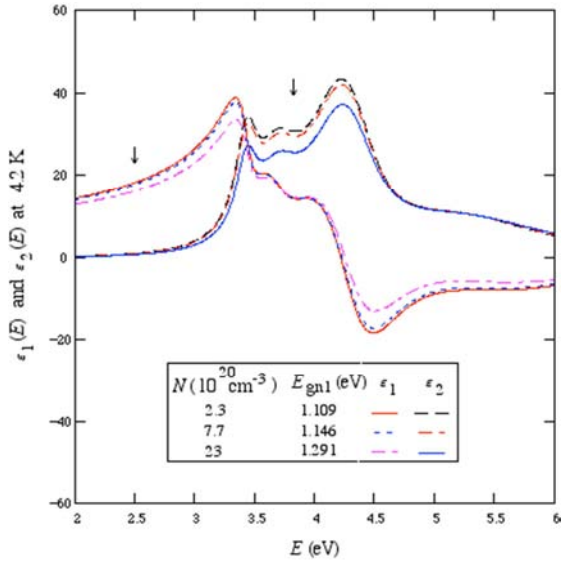

Figure 3c. *In degenerate P-Si systems, our results of* $\varepsilon_{1(2)(IFB-M)}(E)$*, in absolute values, decrease with increasing* N*.*

Finally, in degenerate P-Si systems, in which $\mathbb{E}_{gn} \equiv \mathbb{E}_{gn2}(N)$, being the reduced band gap determined in Eq. (10), decreases with increasing N, due to the heavy-doping effect. Consequently, for a given E, the absolute values of $[E - \mathbb{E}_{gn2}(N)]^2$ and $\varepsilon_{1(2)(IFB-M)}(E)$ increase with increasing N.

Now, identifying our above results (50, 51) and using Eq. (52), we can propose an useful expression for $|v(E)|^2$ as

$$|v(E)|^2 = \frac{\sqrt{2}\times\pi^2\times\hbar\times n_{IFB-M}(E)\times\varepsilon_o\times\mathbb{E}_{Fno}^{3/2}\times f(E)}{q^2\times {m_r}^{3/2}} \times \left(\frac{6\ eV}{E}\right)^3, \text{ for } E \geq 6\ eV,$$

$$= \frac{\sqrt{2}\times\pi^2\times\hbar\times n_{IFB-M}(E)\times\varepsilon_o\times\mathbb{E}_{Fno}^{3/2}\times f(E)}{q^2\times {m_r}^{3/2}}, \text{ for } \mathbb{E}_{gn} \leq E \leq 6\ eV,$$

$$= \frac{\sqrt{2}\times\pi^2\times\hbar\times n_{IFB-M}(\mathbb{E}_{gn})\times\varepsilon_o\times\mathbb{E}_{Fno}^{3/2}\times f(\mathbb{E}_{gn})}{q^2\times {m_r}^{3/2}}, \text{ for } E \leq \mathbb{E}_{gn} \text{ or for } \mathbb{E} \leq 0. \quad (53)$$

6.2. Behaviors of Optical Functions Obtained for $E \leq \mathbb{E}_{gn}$ *or* $\mathbb{E} \leq 0$

Here, going back to the functions: H_n, K_n and F_n, given respectively in Eqs. (26-28) for a=5/2, in which the factor $\frac{\langle \mathbb{E}_k^2 \rangle_{KIM}}{f(a=5/2)}$ is now replaced by: $\frac{\langle \mathbb{E}_k^2 \rangle_{KIM}}{f(a=5/2)} = \frac{\alpha(\mathbb{E}\leq 0)}{\alpha_o(E=\mathbb{E}_{gn})} = F_n(\nu_n, r_d, a = 5/2) \equiv F_{n(\frac{5}{2})}(\nu_n, r_d)$ calculated using Eq. (28), for a simplicity of presentation, $\alpha_o(E = \mathbb{E}_{gn})$ being determined from Eqs. (26, 49, 53) as: $\alpha_o = \frac{f(\mathbb{E}_{gn})\times\eta_n^2(N^*, r_d)}{c\times\hbar\times\mathbb{E}_{gn}}$, then our numerical results of reduced optical absorption coefficient given in degenerate d-Si systems at 0 K and for $N = 5\times10^{20}\ cm^{-3}$, $F_{n(\frac{5}{2})}(\nu_n, r_d)$, are plotted in Figure 4, as functions of ν_n.

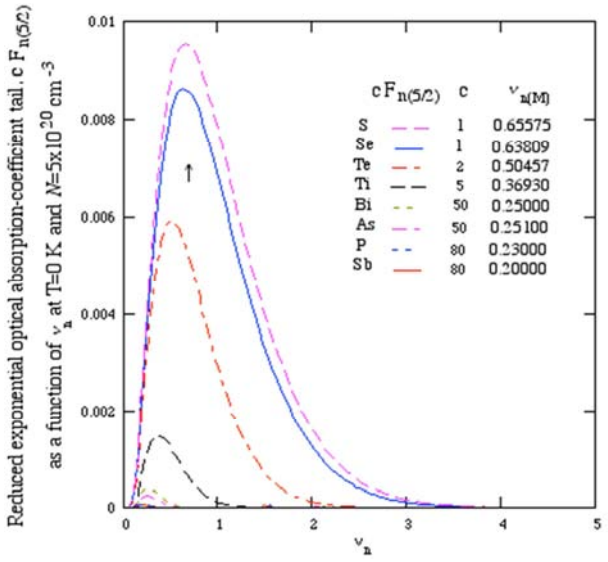

Figure 4. *Our results of $F_{n(\frac{5}{2})}$ increase with increasing r_d for a given ν_n, due to the donor-size effect, and present the maxima at $\nu_n = \nu_{n(M)}$ and go to zero as $\nu_n \to 0$ and ∞.*

Figure 4 shows that:

(i) our results of $F_{n(\frac{5}{2})}$ increase with increasing r_d for a given ν_n, due to the donor-size effect, and

(ii) present the maxima at $\nu_n = \nu_{n(M)}$ and go to zero as $\nu_n \to 0$ and ∞, being found to be in good agreement with theoretical results obtained by Lifshitz [18], Friedberg and Luttinger [20], our results given in Eq. (A.3) of the Appendix A, and in particular with an asymptotic form for exponential conduction-band tail, obtained for $0 \lesssim \nu_n \lesssim \infty$, by Halperin and Lax [19], using the minimum counting methods.

Then, in degenerate d-Si systems at 0 K and $N = 5 \times 10^{20}\ cm^{-3}$, our numerical results of $\ln[F_n(\nu_n, r_d, a = 5/2)] < 0$, which can take its approximate form, obtained in small ν_n -intervals: $\nu_1 \le \nu_n \le \nu_2$, by: $\ln[F_n(\nu_n, r_d, a = 5/2)] \simeq AF(\nu_n, r_d, \nu_1, \nu_2, z, f) = e(r_d, \nu_1, \nu_2, z) \times \nu_n^z + f < 0$, as those given in Eqs. (29, 30), are tabulated in Table 7.

Table 7. *In the d-Si systems at T=0 K and for $N = 5 \times 10^{20}\ cm^{-3}$, using the reduced optical absorption coefficient determined in Eq. (28), $F_n(\nu_n, r_d, a = 5/2)$, the numerical results of $\ln[F_n(\nu_n, r_d, a = 5/2)]$ and its approximate form for a=5/2: $AF(\nu_n, r_d, \nu_1, \nu_2, z, f) = e(r_d, \nu_1, \nu_2, z) \times \nu_n^z + f$, determined in Eqs. (29, 30) for small ν_n-intervals: $\nu_1 \le \nu_n \le \nu_2$, and those of absolute relative errors defined by: $|RE| \equiv 1 - \frac{AF(\nu_n, r_d, \nu_1, \nu_2, z, f)}{\ln[F_n(\nu_n, r_d, a=5/2)]}$, are calculated and tabulated below.*

Donor	**Sb**	**P**	**As**	**Bi**	**Ti**	**Te**	**Se**	**S**
$\nu_{n(M)}$	**0.20000**	**0.23000**	**0.25100**	**0.25000**	**0.36930**	**0.50457**	**0.63809**	**0.65575**
For $1.20 \le \nu_n \le 1.25$, $AF = (e \times \nu_n + f)$ is accurate to within 1.5×10^{-4}, where								
-e	41.048	37.467	22.309	19.884	6.995	2.809	1.455	1.344
f	8.817	7.066	0.610	-0.268	-3.580	-3.690	-3.498	-3.476
$\|RE\|$	1.5×10^{-4}	9.5×10^{-5}	1.4×10^{-4}	8.4×10^{-5}	7.7×10^{-5}	9.4×10^{-5}	7.2×10^{-5}	7.7×10^{-5}
For $1.10 \le \nu_n \le 1.20$, $AF = (e \times \nu_n^{1/2} + f)$ is accurate to within 7.8×10^{-4}, where								
-e	83.727	76.598	45.797	40.849	14.399	5.729	2.905	2.672
f	51.300	46.035	24.020	20.630	3.803	-0.784	-2.061	-2.161
$\|RE\|$	7.8×10^{-4}	7.0×10^{-4}	5.8×10^{-4}	5.6×10^{-4}	3.9×10^{-4}	3.1×10^{-4}	2.7×10^{-4}	2.4×10^{-4}
For $1.07 \le \nu_n \le 1.09$, $AF = (e \times \nu_n^{1/3} + f)$ is accurate to within 6.7×10^{-5}, where								
-e	117.594	107.704	64.640	57.691	20.350	8.001	3.950	3.614
f	84.856	76.863	42.706	37.332	9.706	1.466	-1.031	-1.233
$\|RE\|$	4.0×10^{-5}	4.4×10^{-5}	3.6×10^{-5}	2.7×10^{-5}	5.6×10^{-5}	6.7×10^{-5}	1.1×10^{-5}	1.5×10^{-5}
For $\nu_{n(M)} < 1.00 \le \nu_n \le 1.05$, $AF = (e \times \nu_n^{1/4} + f)$ is accurate to within 2.5×10^{-4}, where								
-e	146.037	133.830	80.538	71.909	25.343	9.835	4.719	4.294
f	113.151	102.853	58.526	51.481	14.674	3.288	-0.269	-0.561
$\|RE\|$	2.5×10^{-4}	2.5×10^{-4}	2.1×10^{-4}	2.0×10^{-4}	1.4×10^{-4}	1.3×10^{-4}	1.7×10^{-4}	7.5×10^{-5}
For $0.090 \le \nu_n \le 0.095 < \nu_{n(M)}$, $AF = (e \times \nu_n^{1/4} + f)$ is accurate to within 2.5×10^{-4}, where								
e	61.911	64.563	73.471	73.821	58.071	40.661	33.954	33.436
f	-51.196	-52.643	-56.888	-56.805	-44.514	-32.149	-27.297	-26.916
$\|RE\|$	2.3×10^{-4}	2.1×10^{-4}	2.5×10^{-4}	2.5×10^{-4}	2.4×10^{-4}	1.6×10^{-4}	1.6×10^{-4}	1.6×10^{-4}
For $0.088 \le \nu_n \le 0.090$, $AF = (e \times \nu_n^{1/3} + f)$ is accurate to within 7.8×10^{-5}, where								
e	61.933	64.532	73.219	73.525	57.271	39.554	32.765	32.240
f	-45.044	-46.203	-49.462	-49.324	-38.375	-27.605	-23.384	-23.052
$\|RE\|$	4.7×10^{-5}	5.4×10^{-5}	6.8×10^{-5}	5.6×10^{-5}	7.5×10^{-5}	3.6×10^{-5}	4.3×10^{-5}	7.8×10^{-5}
For $0.080 \le \nu_n \le 0.083$, $AF = (e \times \nu_n^{1/2} + f)$ is accurate to within 1.5×10^{-4}, where								

Donor	**Sb**	**P**	**As**	**Bi**	**Ti**	**Te**	**Se**	**S**
$\nu_{n(M)}$	**0.20000**	**0.23000**	**0.25100**	**0.25000**	**0.36930**	**0.50457**	**0.63809**	**0.65575**
e	77.110	80.266	90.763	91.957	69.455	46.413	37.693	37.021
f	-40.295	-41.231	-43.731	-43.546	-33.443	-23.746	-19.967	-19.670
|RE|	1.3×10^{-4}	6.7×10^{-4}	1.7×10^{-4}	1.7×10^{-4}	1.5×10^{-4}	1.3×10^{-4}	1.2×10^{-4}	1.1×10^{-4}
For $0.061 \le \nu_n \le 0.064$, AF $= (e\times\nu_n + f)$ is accurate to within 5.1×10^{-4}, where								
e	306.576	319.993	366.932	368.556	267.210	159.872	120.930	117.973
f	-41.333	-42.369	-45.358	-45.205	-33.739	-22.646	-18.456	-18.129
|RE|	3.9×10^{-4}	4.3×10^{-4}	4.9×10^{-4}	5.1×10^{-4}	2.3×10^{-4}	3.2×10^{-4}	2.8×10^{-4}	2.4×10^{-4}
For $0.054 \le \nu_n \le 0.056$, AF $= (e\times\nu_n^2 + f)$ is accurate to within 8.7×10^{-4}, where								
e	4254.38	4420.99	5198.02	5318.51	3719.15	2095.41	1520.14	1476.98
f	-37.877	-38.706	-41.581	-41.708	-30.766	-20.430	-16.560	-16.260
|RE|	3.9×10^{-4}	4.3×10^{-4}	5.5×10^{-4}	8.7×10^{-4}	4.2×10^{-4}	3.0×10^{-4}	2.3×10^{-4}	2.3×10^{-4}

The underlined |RE|-value is the maximal one for each donor-Si system.

Table 7 suggests that: (i) our results of $AF(\nu_n, r_d, \nu_1, \nu_2, z, f)$ given for (z=1)-exponent agree with the Urbach law obtained from linear exponential conduction-band tail-behaviors by some workers [21, 29, 30, 37], (ii) ours for (z=1/2)-exponent and $\nu_n > \nu_{n(M)}$ agree with other theoretical results [19, 37], and finally (iii) ours for (z=1/3, 1/4)-exponents when $\nu_n > \nu_{n(M)}$, and for (z=1/4, 1/3, ½, 1, 2)-exponents when $\nu_n < \nu_{n(M)}$ may thus be new.

Finally, our numerical results of energy parameter, $\mathbb{E}_{no}(N; r_d, a = 5/2)$, obtained in the small interval: $1.2 \le \nu_n \le 1.25$, using Eq. (31), are plotted as functions of N in Figures 5a and 5b, indicating that, for a given N, $\mathbb{E}_{no}$ increases with increasing r_d-values, due to the donor-size effect.

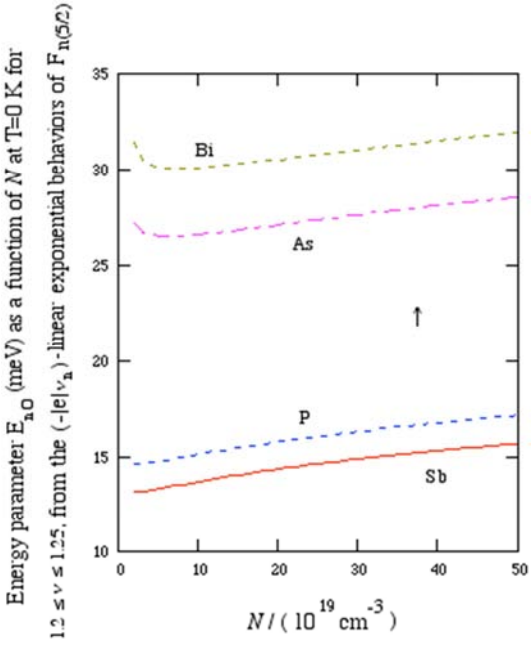

FIG. 5a

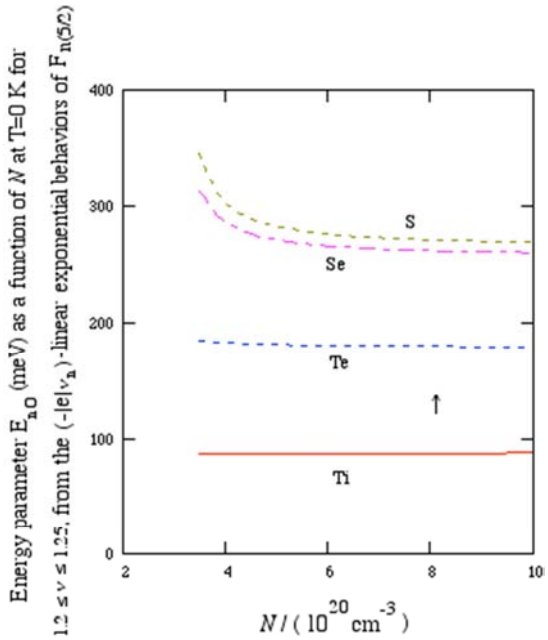

FIG. 5b

Figures 5. *Our results of energy parameter, $\mathbb{E}_{no}(N; r_d, a = 5/2)$ are plotted as functions of N, indicating that, for a given N, $\mathbb{E}_{no}$ increases with increasing r_d-values, due to the donor-size effect.*

7. Electrical Properties

Here, $m^* \equiv m_{cond.} = 0.26 \times m_o$. Then, the electrical functions, obtained in the two cases: $\mathbb{E} \ge 0$ and $\mathbb{E} \le 0$, will be considered as follows.

7.1. Electrical Functions Obtained as $\mathbb{E} \ge 0$

In the effective electron gas at 0 K [66], denoting the relaxation time by τ, the mobility is defined by

$$\mu \equiv \frac{q\times\tau}{m_{cond.}}, \tag{54}$$

the conductivity σ (or resistivity $\rho \equiv 1/\sigma$), given in the Drude model, by

$$\sigma \equiv q \times N \times \mu = q^2 \times N \times \frac{\tau}{m_{cond.}}, \quad (55)$$

the Hall conductivity σ_H, by

$$\sigma_H \equiv -\sigma \times \mu = -\frac{q^3 \times N \times \tau^2}{(m_{cond.})^2} < 0, \quad (56)$$

and finally, from Eqs. (55, 56), the Hall coefficient at 0 K, by

$$R_H(N) \equiv \frac{\langle \sigma_H \rangle}{\langle \sigma \rangle^2} = -\frac{1}{N \times q} \times \frac{\langle \tau^2 \rangle}{\langle \tau \rangle^2} < 0, \frac{\langle \tau^2 \rangle}{\langle \tau \rangle^2} \equiv 1. \quad (57)$$

This result (57) is not correct for the degenerate donor (d)-Si systems at low temperatures, where N may be replaced by the total effective density of free electrons given in the conduction band, $N^* \simeq N - N_{c(d)}$, as that given in Eq. (43), in which the values of critical donor density $N_{c(d)}$ are given in Table I. In those degenerate d-Si systems, the relaxation time can be defined by

$$\frac{1}{\tau(k)} = N^* \times \frac{\hbar k}{m_{cond.}} \times \pi (C \times k)^{-2} \times \prod_{i=1}^{J} x_i \,, \quad (58)$$

where $\hbar k/(m_{cond.} \times m)$ is the electron velocity, C is an empirical parameter, $\pi(C \times k)^{-2}$ is the scattering cross section, and finally the factors x_i are included to represent the high donor-density conditions when $k = k_{Fn}$, as those given in Eq. (14), such that $\frac{1}{\tau(k_{Fn})} < 1$.

We now report and discuss the results of τ, being obtained by Van Cong and Mesnard method (VCMM) [58] and also by Yussouff and Zittarz [59], as follows.

By a Green function (G)-method, assuming that the Gaussian ensemble average of GG as: $\langle GG \rangle \equiv \langle G \rangle \times \langle G \rangle + \Delta G \simeq \langle G \rangle \times \langle G \rangle$, Van Cong and Mesnard obtained [58]

$$\frac{1}{\tau(k_{Fn})} = N^* \times \frac{\hbar k_{Fn}}{m_{cond.}} \times \pi \left(\sqrt{\frac{4\sqrt{\pi}}{3}} \times k_{Fn} \right)^{-2} \times \frac{\eta_n}{\mathbb{E}_{Fno}} < 1, \quad (59)$$

which can be replaced into Eqs. (54, 55), respectively, to obtain

$$\mu_{VCMM} \simeq \frac{4}{3\sqrt{\pi}} \times \frac{q \times k_{Fn}}{N^* \hbar} \times \frac{\mathbb{E}_{Fno}}{\eta_n}, \quad (60)$$

$$\sigma_{VCMM} \simeq \frac{4}{3\sqrt{\pi}} \times \frac{q^2 \times k_{Fn}}{\hbar} \times \frac{\mathbb{E}_{Fno}}{\eta_n}, \quad (61)$$

which is proportional to $\mathbb{E}_{Fno}^{3/2}$, where the Fermi energy $\mathbb{E}_{Fno}(N^*)$ is determined in Eq. (42).

Furthermore, by qualitative arguments, based on the diagram method, then for the lowest order in inverse screening length k_{sn}, Yussouff and Zittarz [59] obtained

$$\frac{1}{\tau(k_{Fn})} = \alpha_{YZ} \times \frac{k_{Fn}^{-1}}{k_{sn}^{-1}} \times \frac{\eta_n}{\mathbb{E}_{Fno}} \times \frac{\eta_n}{\hbar} < 1,$$

where α_{YZ} is the dimensionless function, being not well determined. However, this qualitative argument method is useful to investigate the accurate τ-result, as that given below.

Our numerical calculation indicates that the (μ, σ)-results, obtained from Eqs. (60, 61) do not well agree with the corresponding experimental ones [50, 54, 60]. Thus, there is a need of performing those results.

In this performed VCM-method (PVCMM), proposing the total correction:

$$\Delta_{PVCMM} = -0.01 \times \frac{k_{Fn}^{-1}}{k_{sn}^{-1}} - 0.125 \times \frac{k_{Fn}^{-1}}{a_B(r_d, m_{cond.})},$$

being proportional to $\mathbb{E}_{Fno}^{-1/2}$, where a_B is the effective Bohr radius determined in Eq. (1), and also using our result (34) for $G_p(\mathbb{E}_{Fno}) \equiv \frac{\langle \mathbb{E}^p \rangle_{FDDF}}{\mathbb{E}_{Fno}^p}$ with p=3/2, then the results (60) and (61) are now performed as

$$\mu_{PVCMM}(N^*, T, r_d) \simeq \mu_{VCMM} \times \left\{ G_{\frac{3}{2}}(y) + \Delta_{PVCMM} \times G_1(y) \right\}, \quad (62)$$

$$\sigma_{PVCMM}(N^*, T, r_d) \simeq \sigma_{VCMM} \times \left\{ G_{\frac{3}{2}}(y) + \Delta_{PVCMM} \times G_1(y) \right\}, \quad (63)$$

where μ_{VCMM} and σ_{VCMM} are respectively determined in Eqs. (60, 61) and the function $G_{\frac{3}{2}}(y)$ is given in Table III, with $y = \frac{\pi k_B T}{\mathbb{E}_{Fn}} \simeq \frac{\pi k_B T}{\mathbb{E}_{Fno}}$, noting that $G_1(y) = 1$.

Further, the Hall coefficient is defined by

$$R_{H(PVCMM)}(N^*, T, r_d) \equiv \frac{-\langle \sigma_{PVCMM} \times \mu_{PVCMM} \rangle}{\langle \sigma_{PVCMM} \rangle^2} = -\frac{1}{N^* \times q} \times r_{H(PVCMM)} < 0, \quad (64)$$

where the Hall factor is found to be given by

$$r_{H(PVCMM)}(N^*, T, r_d) \equiv \frac{\langle \tau^2 \rangle}{\langle \tau \rangle^2} = \frac{G_3(y) + \Delta_{PVCMM}^2 \times G_2(y) + 2 \times \Delta_{PVCMM} \times G_{5/2}(y)}{\left(G_{\frac{3}{2}}(y) + \Delta_{PVCMM} \right)^2}. \quad (65)$$

Furthermore, the Hall mobility is given by

$$\mu_{H(PVCMM)}(N^*, T, r_d) = \mu_{PVCMM} \times r_{H(PVCMM)}. \quad (66)$$

We now propose our present method (PM) to determine all the electrical functions as follows.

First of all, one remarks that in Section 6 all the optical functions, given in Eq. (44) and obtained in d-Si systems, are found to be proportional to $\mathbb{E}^2$ or to $\mathbb{E}_{Fno}^2$, as $\mathbb{E} = \mathbb{E}_{Fno}$. Then, in the PM, we propose both principal parts of μ and σ, being

found to be proportional to $\mathbb{E}_{Fno}^2$. Further, using now the total correction given by: $\Delta_{PM} = 0.04 \times \frac{k_{Fn}^{-1}}{k_{sn}^{-1}} + 0.2 \times \frac{k_{Fn}^{-1}}{a_B(r_d, m_{cond.})} - 0.03 \times \sqrt{\frac{\eta_n}{\mathbb{E}_{Fno}}}$, which is proportional to $\mathbb{E}_{Fno}^{-1/2}$, and also using our result (34) for $G_p(\mathbb{E}_{Fno}) \equiv \frac{\langle \mathbb{E}^p \rangle_{FDDF}}{\mathbb{E}_{Fno}^p}$, given for p=2 and p=3/2, we propose the expression for electron mobility, obtained for p=2 and p=3/2, as

$$\mu_{PM}(N^*, T, r_d) \simeq \frac{(0.85)^2}{\pi} \times \frac{q \times k_{Fn}}{N\hbar} \times \frac{a_B}{k_{Fn}^{-1}} \times \frac{k_{sn}^{-1}}{k_{Fn}^{-1}} \times \sqrt{\frac{\mathbb{E}_{Fno}}{\eta_n}} \times \left\{ G_2(y) + \Delta_{PM} \times G_{\frac{3}{2}}(y) \right\}, \quad (67)$$

where $(0.85)^2$ is the empirical parameter chosen to minimize the absolute deviations between the numerical results of μ_{PM} and the corresponding μ-data, and the functions $G_2(y)$ and $G_{\frac{3}{2}}(y)$ are given in Table III. Then, the expression for electrical conductivity is given by

$$\sigma_{PM}(N^*, T, r_d) \simeq \sigma_o(\mathbb{E}_{Fno}) \times \left\{ G_2(y) + \Delta_{PM} \times G_{\frac{3}{2}}(y) \right\}, \quad (68)$$

where $\sigma_o(\mathbb{E}_{Fno}) = \frac{(0.85)^2}{\pi} \times \frac{q^2 \times k_{Fn}}{\hbar} \times \frac{a_B}{k_{Fn}^{-1}} \times \frac{k_{sn}^{-1}}{k_{Fn}^{-1}} \times \sqrt{\frac{\mathbb{E}_{Fno}}{\eta_n}}$, being proportional to $\mathbb{E}_{Fno}^2$.

Further, the Hall coefficient is defined by

$$R_{H(PM)}(N^*, T, r_d) \equiv \frac{-\langle \sigma_{PM} \times \mu_{PM} \rangle}{\langle \sigma_{PM} \rangle^2} = -\frac{1}{N^* \times q} \times r_{H(PM)} < 0, \quad (69)$$

where the Hall factor is given by

$$r_{H(PM)}(N^*, T, r_d) \equiv \frac{\langle \tau^2 \rangle}{\langle \tau \rangle^2} = \frac{G_4(y) + \Delta_{PM}^2 \times G_3(y) + 2 \times \Delta_{PM} \times G_{7/2}(y)}{[G_2(y) + \Delta_{PM} \times G_{3/2}(y)]^2}. \quad (70)$$

Furthermore, the Hall mobility yields

$$\mu_{H(PM)}(N^*, T, r_d) = \mu_{PM} \times r_{H(PM)}. \quad (71)$$

Our numerical calculation indicates that in degenerate d-Si systems the r_H-behaviors obtained in PVCMM and PM, using Eqs. (65, 70), are almost the same. So, in the PM, our numerical results of Hall factors r_H obtained in various d-Si systems at 77 K, using Eq. (70), are plotted as functions of N in Figures 6a and 6b.

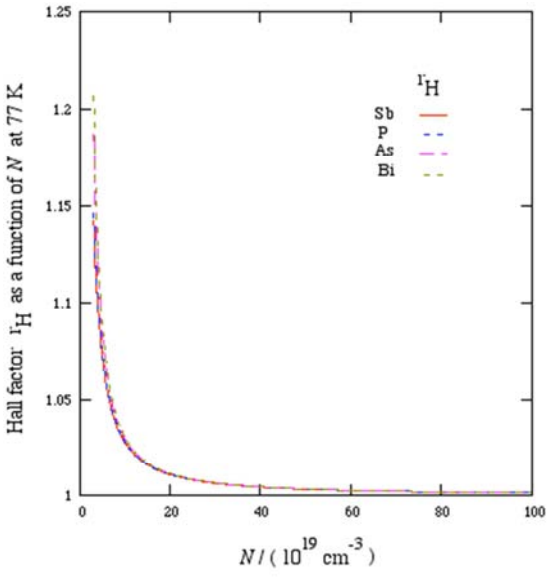

FIG. 6a

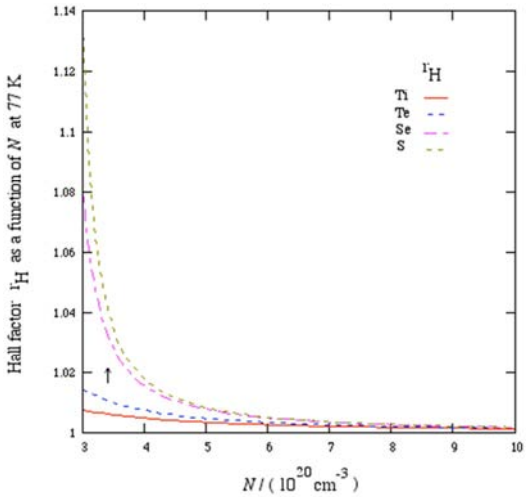

FIG. 6b

Figures 6. *In the PM, our results of Hall factors r_H obtained in various d-Si systems are plotted as functions of N, decreasing with increasing N, increasing with increasing r_d for a given N, and tend towards 1 at very high N.*

Figures 6a and 6b indicate that those results of r_H are positive, decrease with increasing N, increase with increasing r_d for a given N, and tend towards 1 at very high values of N, in good agreement with the result obtained in an effective electron gas [66].

Then, in particular, in the As-Si system at T=10 K and for $N = 2.7 \times 10^{19}$ cm^{-3}, the numerical results of Hall coefficient, $|R_H(N^*)|$, where $N^* \equiv N - N_{c(As)}$, $N_{c(As)} = 8.58 \times 10^{18}$ cm^{-3}, and Hall mobility, $\mu_H(N^*)$, obtained using Eqs. (64, 66) for the PVCMM, and Eqs. (69, 71) for the PM, and their absolute relative errors, |REs|, calculated using the corresponding data obtained by Morin and Maita [50], are tabulated in Table 8.

Table 8. *In the As-Si system at T=10 K and for $N = 2.7 \times 10^{19}$ cm^{-3}, the numerical results of Hall mobility $\mu_H(N^*)$ and Hall coefficient $|R_H(N^*)|$, obtained in the PM and PVCMM, and their absolute relative errors, |REs|, calculated using the corresponding data obtained by Morin and Maita [50], $\mu_{H(data)} = 155$ $(\frac{cm^2}{V \times sec.})$ and $|R_{H(data)}| = 0.33$ (cm^3/C), are calculated and tabulated.*

PM	μ_H [|RE|]	$\|R_H\|$ [|RE|]	PVCMM	μ_H [|RE|]	$\|R_H\|$ [|RE|]
	129.2	0.340		156.5	0.340
	[0.17]	[0.03]		[0.01]	[0.03]

Table 8 indicates |REs| of $\mu_H(N^*)$ and $|R_H(N^*)|$ are equal to 17% and 3% obtained for the PM, and 0.6% and 3% for PVCMM, respectively, confirming thus the use of N^* for the effective density of free electrons given in the conduction band when $N > N_{c(d)}$, given in Eq. (43).

In the P (As)-Si systems at T=4.2 K, $N_{c(P)} = 3.52 \times 10^{18}\ cm^{-3}$ and $N_{c(As)} = 8.58 \times 10^{18}\ cm^{-3}$, as given in Table 1, the numerical results of resistivity $\rho(N^*) = 1/\sigma(N^*)$, $\sigma(N^*)$ being determined in Eq. (63) for the PVCMM and in Eq. (68) for the PM, are tabulated in Table 9, in which their absolute relative errors |REs|, calculated using the data obtained by Chapman et al. [54], are also included, suggesting that the maximal |REs| of $\rho(N^*)$ are equal to 10% (11%), obtained respectively for the PM (PVCMM).

Table 9. *In the P (As)-Si systems at T=4.2 K, the numerical results of resistivity $\rho(N^*)$, obtained for the PM and PVCMM and expressed in $[10^{-4}\ ohm \times cm]$, are tabulated in this Table IX, in which their absolute relative errors $|REs|$, calculated using the data obtained by Chapman et al. [54], are also included, suggesting that the maximal $|REs|$ of $\rho(N^*)$ are equal to 10% (11%), obtained respectively for the PM (PVCMM).*

N (10^{19} cm^{-3})	**1.1**	**1.6**	**2.7**	**3.9**	**5**	**7**	**13**
$\rho_{Exp.}$ (donor)	**33 (P)**	**23 (P)**	**13 (P)**	**9.4 (P)**	**13 (As)**	**6 (P)**	**3.8 (P)**
In the PM, the results of ρ are accompanied by their AREs as:							
ρ(N*) (|RE|)	35.8 (0.08)	23.9 (0.04)	14.5 (0.10)	10.4 (0.10)	13.9 (0.07)	6.2 (0.03)	3.6 (0.05)
In the PVCMM, the results of ρ are accompanied by their AREs as:							
ρ(N*) (|RE|)	29.5 (0.10)	20.5 (0.11)	13.2 (0.01)	9.9 (0.05)	12.3 (0.06)	6.5 (0.08)	4.2 (0.11)

The underlined $|RE|$-value is the maximal one.

In the P-Si system at T=77 K and for $N_{c(P)} = 3.52 \times 10^{18}\ cm^{-3}$, the numerical results of conductivity $\sigma(N^*)$, obtained respectively from Eqs. (63, 68) for the PVCMM and PM, are tabulated in this Table 10, in which their absolute relative errors |REs|, calculated using the σ-data obtained by Finetti and Mazzone [60], are also included. This indicates that the maximal |RE| of $\sigma(N^*)$ are equal to 12% and 14% for PM and PVCMM, respectively.

Table 10. *In the P-Si system at T=77 K, the numerical results of conductivity $\sigma(N^*)$, obtained respectively for the PVCMM and PM, are tabulated in this Table X, in which their absolute relative errors $|REs|$, calculated using the σ-data obtained by Finetti and Mazzone [60], are also included, indicating that its maximal $|REs|$ are equal to 12% and 14% for PM and PVCMM, respectively.*

N (10^{19} cm^{-3})	**1.85**	**5.55**	**8.65**
σ_{data}(ohm^{-1} × cm^{-1})	**559**	**1500**	**2000**
In the PM, the results of σ are accompanied by their |REs| as:			
σ(N*) (|RE|)	520 (0.07)	1339 (0.12)	1962 (0.02)
In the PVCMM, the results of σ are accompanied by their |REs| as:			
σ(N*) (|RE|)	575 (0.03)	1318 (0.14)	1799 (0.11)

The underlined $|RE|$-value is the maximal one.

As noted above, in the following, we will only present the numerical results of various electrical and thermoelectric functions obtained in the PM, since those obtained in the PVCMM can also be investigated by a same treatment.

In the degenerate d-Si systems at 77 K, the numerical results of resistivity $\rho(N^*, T, r_d) = 1/\sigma(N^*, T, r_d)$, $\sigma(N^*, T, r_d)$ being calculated from Eq. (68), and those of mobility $\mu(N^*, T, r_d)$ and Hall mobility $\mu_H(N^*, T, r_d)$ obtained respectively from Eqs. (67, 71), are tabulated in Tables 11 and 12.

Table 11. *In the degenerate d-Si systems at 77 K, the numerical results of resistivity $\rho(N^*, T, r_d)$ are expressed in $10^{-4} ohm \times cm$.*

Donor	**Sb**	**P**	**As**	**Bi**	**Ti**	**Te**	**Se**	**S**
***N* (10^{19} cm^{-3})**	**ρ**	**ρ**	**ρ**	**ρ**	**ρ**	**ρ**	**ρ**	**ρ**
3	11.58	12.68	22.37	25.92				
6	6.40	6.98	11.56	12.97				
10	4.12	4.49	7.32	8.14				
40	1.22	1.33	2.18	2.41	5.75	12.41	24.69	27.23
70	0.74	0.81	1.33	1.48	3.48	6.70	10.22	10.70
100	0.53	0.58	0.97	1.08	2.54	4.74	6.81	7.06

Table 12. *In the degenerate d-Si systems at 77 K, the numerical results of mobility $\mu(N^*, T, r_d)$ and Hall mobility $\mu_H(N^*, T, r_d)$, both expressed in $(\frac{cm^2}{V.sec})$ and obtained respectively from Eqs. (67, 71), are tabulated here. This indicates that $\mu_H = \mu$ at $N = 10^{21}\ cm^{-3}$.*

Donor	**Sb**	**P**	**As**	**Bi**	**Ti**	**Te**	**Se**	**S**
N (10^{19} cm^{-3})	**μ (μ$_H$)**	**μ (μ$_H$)**	**μ (μ$_H$)**	**μ (μ$_H$)**	**μ (μ$_H$)**	**μ (μ$_H$)**	**μ (μ$_H$)**	**μ (μ$_H$)**
3	200 (228)	186 (213)	130 (155)	123 (148)				
6	171 (180)	158 (167)	105 (111)	97 (103)				
10	156 (160)	144 (148)	93 (96)	85 (88)				
40	129 (129)	118 (119)	73 (74)	66 (67)	31 (31)	20 (20)	18 (18)	18 (18)
70	121 (122)	111 (111)	68 (68)	61 (61)	28 (28)	17 (17)	14 (14)	14 (14)
100	117 (117)	107 (107)	65 (65)	59 (59)	26 (26)	15 (15)	12 (12)	12 (12)

Table 11 indicates that (i) at a given r_d, the resistivity decreases with increasing N, and (ii) at a given N, it increases with increasing r_d. That means: $\rho(r_{Sb}) < \rho(r_P) < \rho(r_{As}) < \cdots < \rho(r_{Se}) < \rho(r_S)$, in good agreement with the observations by Logan et al. [53].

Table 12 suggests that (i) for a given r_d, the mobility and the Hall mobility decrease with increasing N, (ii) for given N, they decrease with increasing r_d, since μ (or μ_H) is proportional to $\sigma \equiv 1/\rho$, where ρ increases with increasing r_d, as observed in above Table XI, (iii) for given N and r_d,

$\mu_H > \mu$, and finally $\mu_H = \mu$ for $N = 10^{21}$ cm^{-3}, since the Hall factor r_H is equal to 1, as that given in the effective electron gas [66].

Now, in degenerate (d)-Si systems at 77 K, from the generalized Einstein relation [62-67], it is interesting to present in following Table 13 our numerical results of diffusion coefficients: $D(N^*, T, r_d)$, $D_o(N^*, T, r_d)$, and $D_1(N^*, T, r_d)$, determined respectively in Eqs. (A15, A16, A17) of the Appendix C, being related to the mobility $\mu(N^*, T, r_d)$ given in Eq. (67).

Table 13. *In degenerate (d)-Si systems at 77 K, our numerical results of diffusion coefficients ($\frac{cm^2}{sec}$): D, D_o, and D_1 determined respectively in Eqs. (A15, A16, A17) of the Appendix C, being related to the mobility μ determined in Eq. (67), are tabulated here.*

Donor	**Sb**	**P**	**As**	**Bi**	**Ti**	**Te**	**Se**	**S**
N	**D (D_1)**	**D (D_1)**	**D (D_1)**	**D (D_1)**	**D (D_1)**	**D (D_1)**	**D (D_1)**	**D (D_1)**
3	5.795	(5.793)	5.290	(5.288)	3.074	(3.069)	2.701	(2.695)
6	8.264	(8.266)	7.559	(7.560)	4.539	(4.539)	4.049	(4.049)
10	10.873	(10.876)	9.947	(9.949)	6.036	(6.037)	5.415	(5.416)
40	23.587 (23.593)	21.523 (21.528)	13.004 (13.007)	11.697 (11.699)	4.808 (4.809)	2.295 (2.296)	1.282 (1.282)	1.187 (1.187)
70	32.576 (32.583)	29.684 (29.691)	17.809 (17.813)	16.000 (16.004)	6.629 (6.630)	3.433 (3.434)	2.310 (2.310)	2.216 (2.217)
100	40.129 (40.138)	36.535 (36.544)	21.814 (21.819)	19.579 (19.584)	8.097 (8.099)	4.293 (4.294)	3.014 (3.015)	2.911 (2.912)
N	D_o	D_o	D_o	D_o	D_o	D_o	D_o	D_o
100	40.127	36.534	21.812	19.578	8.096	4.292	3.013	2.910

Table 13 indicates that: (i) for a given r_d, D and D_1 increase with increasing N, (ii) for a given N, since D, D_1 and μ, being expressed in terms of $\sigma \equiv 1/\rho$, where ρ increases with increasing r_d, as observed in above Table 11, our results of D and D_1 thus decrease with increasing r_d, due to the donor-size effect, and finally (iii) for $N = 10^{21}$ cm^{-3}, all the results of D, D_1 and D_o are found to be almost the same, suggesting that the asymptotic behaviors of D and D_1 are correct.

7.2. Behaviors of Electrical Functions Obtained for $\mathbb{E} \leq 0$

First of all, it should be noted from Eqs. (26, 68) that for any $\mathbb{E}$ the conductivity can be rewritten in a general form as

$$\sigma_{PM}(\mathbb{E}, r_d) \equiv \sigma(\mathbb{E}, r_d) \simeq \sigma_o(\mathbb{E}_{Fno}) \times \left\{\frac{\langle E_k^2\rangle_{KIM}}{\mathbb{E}_{Fno}^2} + \Delta_{PM} \times \frac{\langle E_k^{3/2}\rangle_{KIM}}{\mathbb{E}_{Fno}^{3/2}}\right\}, \quad (72)$$

where $\sigma_o(\mathbb{E}_{Fno}) = \frac{(0.85)^2}{\pi} \times \frac{q^2 \times k_{Fn}}{\hbar} \times \frac{a_B}{k_{Fn}^{-1}} \times \frac{k_{sn}^{-1}}{k_{Fn}^{-1}} \times \sqrt{\frac{\mathbb{E}_{Fno}}{\eta_n}}$ is proportional to $\mathbb{E}_{Fno}^2$, and $\langle E_k^{a-\frac{1}{2}}\rangle_{KIM}$ is determined in Eq. (26) for a = 5/2 and a= 2, respectively.

Here, as $\mathbb{E} \leq 0$, using the functions: H_n, K_n and F_n, given respectively in Eqs. (26-28) for a=5/2 and 2, the conductivity, given in Eq. (72), is now rewritten by

$$\sigma(\nu_n, r_d) \simeq \frac{\sigma_o(\mathbb{E}_{Fno})}{\sqrt{2\pi}} \times \left\{\frac{\Gamma(3)\times\beta(\frac{5}{2})}{A_n^2} \times F_n(a = 5/2) + \Delta_{PM} \times \frac{\Gamma(5/2)\times\beta(2)}{A_n^{3/2}} \times F_n(a = 2)\right\}, A_n \equiv \frac{\mathbb{E}_{Fno}}{\eta_n}. \quad (73)$$

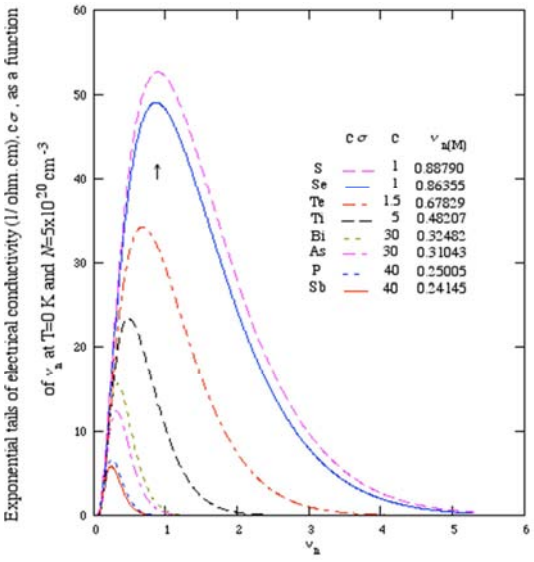

Figure 7. *Our results of electrical conductivity $\sigma(\nu_n, r_d)$ increase with increasing r_d for a given ν_n, due to the donor-size effect, and present the maxima at $\nu_n = \nu_{n(M)}$ and go to zero as $\nu_n \to 0$ and ∞.*

So, our numerical results of exponential tails of the electrical conductivity $\sigma(\nu_n, r_d)$ at 0 K and for $N = 5 \times 10^{20}$ cm^{-3}, calculated using Eq. (73), are plotted in Figure 7, as functions of ν_n.

Figure 7 shows that:

(i) our results of $\sigma(\nu_n, r_d)$ increase with increasing r_d for a given ν_n, due to the donor-size effect, and

(ii) present the maxima at $\nu_n = \nu_{n(M)}$ and go to zero as $\nu_n \to 0$ and ∞, being found to be in good agreement with theoretical results obtained by Lifshitz [18], Friedberg and Luttinger [20], our results given in Eq. (A.3) of the Appendix A, and in particular with an asymptotic form for exponential conduction-band tail, obtained for $0 \lesssim \nu_n \lesssim \infty$, by Halperin and Lax [19], using the minimum counting methods.

Further, our numerical results of the function $\ln[\sigma(\nu_n, r_d)] < 0$, which can take its approximate form as: $\ln[\sigma(\nu_n, r_d)] \simeq AF(\nu_n, r_d, \nu_1, \nu_2, z, f) = e(r_d, \nu_1, \nu_2, z) \times \nu_n^z + f < 0$, are evaluated in small ν_n-intervals: $\nu_1 \leq \nu_n \leq \nu_2$, using Eq. (29) and Eq. (30), being now defined as: $e(r_d, \nu_1, \nu_2, z) \equiv \frac{\ln[\sigma(\nu_2, r_d)] - \ln[\sigma(\nu_1, r_d)]}{\nu_2^z - \nu_1^z}$, are tabulated in Table 14.

Table 14. *In the d-Si systems at T=0 K and for $N = 5 \times 10^{20}\ cm^{-3}$, using the expression for electrical conductivity determined in Eq. (73), $\sigma(\nu_n, r_d)$, the numerical results of $ln[\sigma(\nu_n, r_d)]$ and its approximate form: $AF(\nu_n, r_d, \nu_1, \nu_2, z, f) = e(r_d, \nu_1, \nu_2, z) \times \nu_n^z + f$, determined in Eq. (29) for small ν_n-intervals: $\nu_1 \leq \nu_n \leq \nu_2$, and those of absolute relative errors: $|RE| \equiv 1 - \frac{AF(\nu_n, r_d, \nu_1, \nu_2, z, f)}{ln[\sigma(\nu_n, r_d)]}$, are evaluated and tabulated below.*

Donor	**Sb**	**P**	**As**	**Bi**	**Ti**	**Te**	**Se**	**S**
$\nu_{n(M)}$	**0.24145**	**0.25005**	**0.31043**	**0.32482**	**0.48207**	**0.67829**	**0.86355**	**0.88790**
For $1.37 \leq \nu_n \leq 1.42$, AF = $(e \times \nu_n + f)$ is accurate to within 1.9×10^{-3}, where								
-e	17.734	16.287	9.955	8.926	3.291	1.330	0.655	0.597
f	9.234	8.507	5.708	5.338	4.140	4.385	4.602	4.618
|RE|	1.2×10^{-4}	1.2×10^{-4}	1.0×10^{-4}	1.2×10^{-4}	1.9×10^{-3}	2.4×10^{-4}	1.2×10^{-4}	1.2×10^{-4}
For $1.28 \leq \nu_n \leq 1.30$, AF = $(e \times \nu_n^{1/2} + f)$ is accurate to within 1.5×10^{-3}, where								
-e	38.134	35.052	21.508	19.293	7.088	2.792	1.300	1.173
f	29.621	27.264	17.269	15.714	7.937	5.835	5.229	5.177
|RE|	4.7 ×10−5	4.8×10^{-5}	1.2×10^{-4}	4.7×10^{-5}	1.5×10^{-3}	6.2×10^{-5}	3.1×10^{-5}	1.3×10^{-4}
For $1.180 \leq \nu_n \leq 1.185$, AF = $(e \times \nu_n^{1/3} + f)$ is accurate to within 9.4×10^{-4}, where								
-e	53.080	48.832	30.060	26.972	9.829	3.722	1.582	1.400
f	44.192	40.703	25.620	23.212	10.606	6.726	5.482	5.375
|RE|	3.2×10^{-5}	2.7×10^{-5}	7.1×10^{-5}	9.0×10^{-5}	9.4×10^{-4}	1.5×10^{-4}	5.5×10^{-5}	1.7×10^{-5}
For $\nu_{n(M)} < 1.155 \leq \nu_n \leq 1.165$, AF = $(e \times \nu_n^{1/4} + f)$ is accurate to within 1.4×10^{-3}, where								
-e	69.838	64.260	39.580	35.514	12.909	4.837	2.003	1.761
f	60.894	56.079	35.109	31.727	13.674	7.834	5.898	5.731
|RE|	4.1×10^{-5}	1.8×10^{-5}	6.9×10^{-5}	6.7×10^{-5}	1.4×10^{-3}	6.8×10^{-5}	1.8×10^{-5}	7.9×10^{-5}
For $0.110 \leq \nu_n \leq 0.115 < \nu_{n(M)}$, AF = $(e \times \nu_n^{1/4} + f)$ is accurate to within 2.1×10^{-3}, where								
e	26.262	27.342	31.423	31.800	28.839	23.832	21.614	21.434
f	-18.507	-19.124	-21.180	-21.273	-17.859	-13.499	-11.563	-11.406
|RE|	2.8×10^{-4}	1.5×10^{-4}	5.3×10^{-4}	4.9×10^{-4}	8.2×10^{-4}	2.1×10^{-3}	8.3×10^{-4}	4.3×10^{-4}
For $0.088 \leq \nu_n \leq 0.090$, AF = $(e \times \nu_n^{1/3} + f)$ is accurate to within 4.3×10^{-3}, where								
e	37.452	38.777	43.541	43.855	37.449	29.015	25.442	25.153
f	-21.105	-21.729	-23.698	-23.724	-19.008	-13.555	-11.210	-11.021
|RE|	9.5×10^{-5}	1.4×10^{-4}	9.7×10^{-5}	1.6×10^{-4}	3.0×10^{-4}	4.1×10^{-4}	4.3×10^{-3}	9.5×10^{-4}
For $0.070 \leq \nu_n \leq 0.073$, AF = $(e \times \nu_n^{1/2} + f)$ is accurate to within 1.6×10^{-3}, where								
e	59.884	62.021	69.660	70.074	57.026	41.116	34.641	34.124
f	-21.865	-22.520	-24.590	-24.595	-18.965	-12.661	-10.030	-9.820
|RE|	3.6×10^{-4}	3.9×10^{-4}	4.5×10^{-4}	7.5×10^{-4}	8.9×10^{-4}	6.1×10^{-4}	1.6×10^{-3}	9.2×10^{-4}
For $0.061 \leq \nu_n \leq 0.064$, AF = $(e \times \nu_n + f)$ is accurate to within 1.5×10^{-3}, where								
e	162.658	168.842	191.433	192.696	152.729	104.514	85.401	83.890
f	-17.234	-17.750	-19.349	-19.334	-14.409	-9.005	-6.774	-6.597
|RE|	5.9×10^{-4}	6.7×10^{-4}	7.3×10^{-4}	6.9×10^{-4}	8.3×10^{-4}	9.3×10^{-4}	1.1×10^{-3}	1.5×10^{-3}
For $0.054 \leq \nu_n \leq 0.056$, AF = $(e \times \nu_n^2 + f)$ is accurate to within 9.9×10^{-4}, where								
e	2147.35	2236.99	2576.10	2597.50	2013.29	1302.33	1027.98	1006.55
f	-15.033	-15.491	-16.923	-16.906	-12.330	-7.329	-5.282	-5.120
|RE|	5.4×10^{-4}	5.2×10^{-4}	6.5×10^{-4}	6.2×10^{-4}	6.6×10^{-4}	8.6×10^{-4}	8.8×10^{-4}	9.9×10^{-4}

The underlined $|RE|$-value is the maximal one for each donor-Si system.

Table 14 suggests that: (i) our results of $AF(\nu_n, r_d, \nu_1, \nu_2, z, f)$ given for (z=1)-exponent agree with the Urbach law obtained from linear exponential conduction-band tail-behaviors by some workers [21, 29, 30, 37], (ii) ours for (z=1/2)-exponent and $\nu_n > \nu_{n(M)}$ agree with other theoretical results [19, 37], and finally (iii) ours for (z=1/3, 1/4)-exponents when $\nu_n > \nu_{n(M)}$, and for (z=1/4, 1/3, ½, 1, 2)-exponents when $\nu_n < \nu_{n(M)}$ may thus be new.

Finally, our numerical results of energy parameter, $\mathbb{E}_{no}(N; r_d)$, obtained in the small interval: $1.37 \leq \nu_n \leq 1.42$, using Eq. (31), are plotted as functions of N in Figures 8a and 8b, indicating that, for a given N, $\mathbb{E}_{no}$ increases with

increasing r_d-values, due to the donor-size effect.

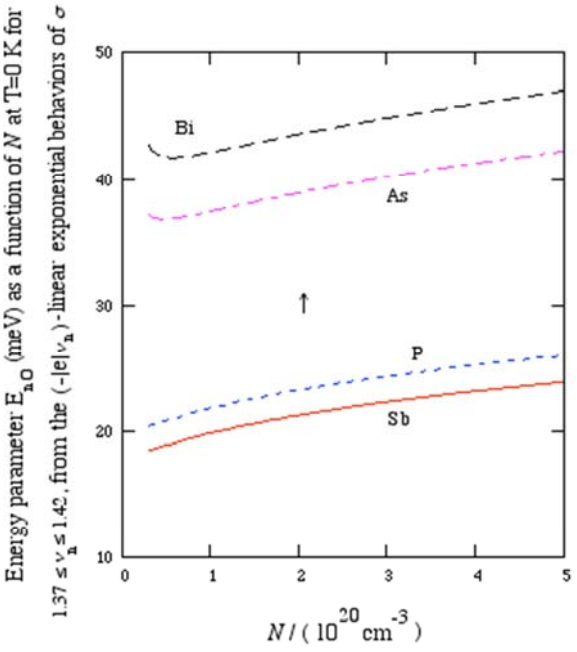

FIG. 8a

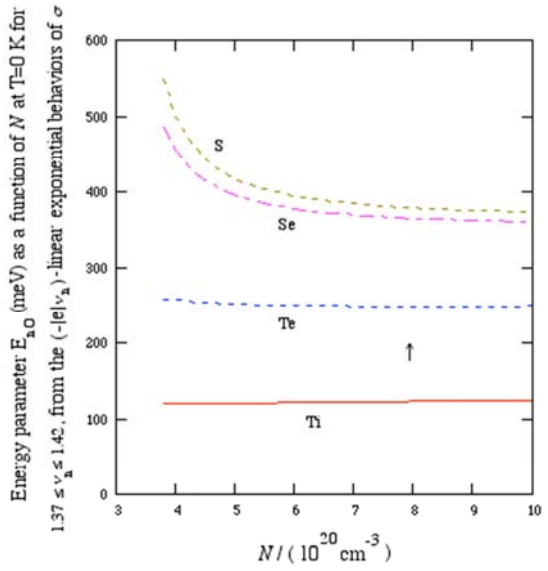

FIG. 8b

Figures 8. *Our results of energy parameter, $\mathbb{E}_{no}(N; r_d)$, are plotted as functions of N, indicating that, for a given N, $\mathbb{E}_{no}$ increases with increasing r_d-values, due to the donor-size effect.*

8. Thermoelectric Properties

When the electron-electron and electron-phonon interactions are neglected, the Kubo formulae for the thermal transport coefficients [51], derived by very general arguments of Luttinger [55], are found to be reduced to the Greenwood ones [52]. Then, the phenomenological equations are written as [58]

$$\vec{J}(\vec{r}) = L^{(1)} \times \vec{\mathcal{E}} + L^{(2)} \times T \times \vec{\nabla}(T^{-1}), \tag{74}$$

$$\vec{J^{\mathbb{E}}}(\vec{r}) = L^{(3)} \times \vec{\mathcal{E}} + L^{(4)} \times T \times \vec{\nabla}(T^{-1}), \tag{75}$$

where $\vec{J}$ is the electric current density, $\vec{J^{\mathbb{E}}}$ is the energy current, $\vec{\mathcal{E}}$ is the electric field, and $L^{(i)}$ is the transport coefficient determined in an isotropic system. Now, using the average of $\langle \mathbb{E}^p \rangle_{FDDF} \equiv G_p(y) \times \mathbb{E}_{Fno}^p$, where the expressions for $G_p(y)$, $y = \frac{\pi k_B T}{\mathbb{E}_{Fn}} \simeq \frac{\pi k_B T}{\mathbb{E}_{Fno}}$, are determined in Eq. (34) and given in Table III, calculated using the Fermi-Dirac distribution function (FDDF), and using also the expression for electrical conductivity as a function of $\mathbb{E}$, derived from Eq. (72) for $\mathbb{E} \geq 0$, as

$$\sigma(\mathbb{E}, r_d) \simeq \sigma_o(\mathbb{E}_{Fno}) \left\{ \frac{\mathbb{E}^2}{\mathbb{E}_{Fno}^2} + \Delta_{PM} \times \frac{\mathbb{E}^{3/2}}{\mathbb{E}_{Fno}^{3/2}} \right\}, \tag{76}$$

the Onsager relations are found to be given as follows.

First, one has [58, 61]

$$L^{(1)} \equiv \langle \sigma(\mathbb{E}, r_d) \rangle_{FDDF} = \sigma_o(\mathbb{E}_{Fno}) \left\{ \frac{\langle \mathbb{E}^2 \rangle_{FDDF}}{\mathbb{E}_{Fno}^2} + \Delta_{PM} \times \frac{\langle \mathbb{E}^{3/2} \rangle_{FDDF}}{\mathbb{E}_{Fno}^{3/2}} \right\},$$

$$= \sigma_o(\mathbb{E}_{Fno}) \left\{ G_2(y) + \Delta_{PM} \times G_{\frac{3}{2}}(y) \right\}, \tag{77}$$

which is just the result obtained in Eq. (68).

Then, one gets [58]

$$L^{(2)} = L^{(3)} = -\frac{1}{q} \times \langle \mathbb{E} \times \sigma(\mathbb{E}, r_d) \rangle_{FDDF} = -\frac{\sigma_o(\mathbb{E}_{Fno})}{q} \times \left\{ G_3(y) + \Delta_{PM} \times G_{\frac{5}{2}}(y) \right\}. \tag{78}$$

Finally, one obtains [58]

$$L^{(4)} = \frac{1}{q^2} \times \langle \mathbb{E}^2 \times \sigma(\mathbb{E}, r_d) \rangle_{FDDF} = \frac{\sigma_o(\mathbb{E}_{Fno})}{q^2} \times \left\{ G_4(y) + (\Delta\sigma)_{PM} \times G_{\frac{7}{2}}(y) \right\}. \tag{79}$$

Now, from Eqs. (77-79), one can define the thermal conductivity by [58, 61]

$$K_T(N^*, T, r_d) \equiv \frac{1}{T} \times \left\{ L^{(4)} - \frac{[L^{(2)}]^2}{L^{(1)}} \right\}. \tag{80}$$

Some remarks obtained from Eq. (80) are given as follows.

(i) First, our numerical calculation indicates that, in the degenerate (P)-Si system, for $N = 10^{21}$ cm^{-3} and at T=3 K and 300 K, noting that at 300 K the degenerate temperature T_D is equal to 7895 K $\gg$ 300 K, our results of K_T are equal to 8×10^{-4} and 0.125 W/(cm.K), in good agreement with the experimental results obtained by Slack [68]: 5×10^{-4} and between 0.1 and 0.2 W/(cm.K), respectively.

(ii) Second, at $N = 10^{21}$ cm^{-3} and T=3 K, the values of relative deviations between our results of $K_T(N^*, T, r_d)/[T \times \sigma(N^*, T, r_d)]$, calculated using Eqs. (68) and (80), and the constant: $\frac{\pi^2}{3}\left(\frac{k_B}{q}\right)^2 = 2.443 \times 10^{-8}$ W.Ω.K^{-2}, being obtained from the Wiedemann-Frank law for metals [58, 61], are tabulated in Table 15, indicating that our result (80) well verifies this law, with a precision of the order of 6.52×10^{-7}.

Table 15. *For $N = 10^{21}\ cm^{-3}$ and T=3 K, the values of the relative deviations (RD) between our results of $\frac{K_T}{T\times\sigma}$ obtained in various degenerate donor-Si systems, and the constant: $\frac{\pi^2}{3}\left(\frac{k_B}{q}\right)^2 = 2.443\times10^{-8}\ W.\Omega.K^{-2}$, obtained from the Wiedemann-Frank law for metals, indicating a perfect agreement between those results.*

Donor	Sb	P	As	Bi	Ti	Te	Se	S
RE	4.72×10^{-7}	-9.40×10^{-8}	-3.51×10^{-8}	3.79×10^{-7}	1.67×10^{-7}	-6.52×10^{-7}	-1.53×10^{-7}	-5.95×10^{-8}

The underlined $|RE|$-value is the maximal one for each donor-Si system.

(iii) Finally, our numerical calculation shows that, in degenerate (d)-Si systems, for $N = 10^{21}\ cm^{-3}$ and in the temperature range from T=3 to 300 K, the maximal value of absolute deviations between $K_T(N^*, T, r_d)$ given in Eq. (80) and its approximate form $K_T(N^*, T, r_d) \simeq C_{K_T} \times T$ is found to be equal to 9.9×10^{-4}, in good agreement with our previous result [58, 61]. Then, those are plotted in Figure 9a as functions of T, suggesting that at a given T the thermal conductivity K_T decreases with increasing r_d, due to the donor-size effect.

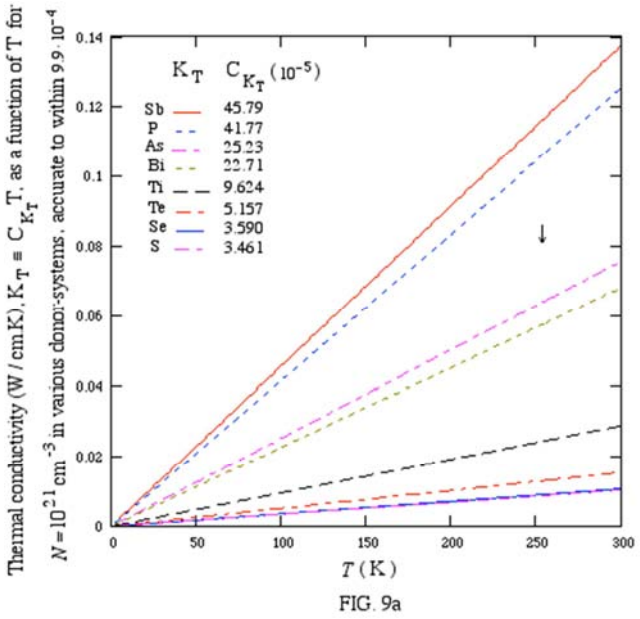

Figure 9a. *Our results of $K_T(N^*, T, r_d) \simeq C_{K_T} \times T$ are plotted as functions of T, suggesting that at a given T the thermal conductivity K_T decreases with increasing r_d, due to the donor-size effect.*

Then, from Eqs. (77, 78) for $L^{(1)}$ and $L^{(2)}$, and Eq. (D1) of the Appendix D for $\mathbb{E}_{Fn}$, the absolute thermoelectric power Q can be defined by [58, 61]

$$Q(N^*, T, r_d) \equiv \frac{1}{T} \times \left\{\frac{L^{(2)}}{L^{(1)}} + \frac{\mathbb{E}_{Fn}}{q}\right\}. \quad (81)$$

This result (81) is a function commonly used to describe the following thermoelectric coefficients [58, 61], such as: the Thomson coefficient,

$$T_S(N^*, T, r_d) \equiv T \times \frac{dQ(N^*, T, r_d)}{dT}, \quad (82)$$

the Peltier coefficient,

$$P_T(N^*, T, r_d) \equiv -T \times Q(N^*, T, r_d), \quad (83)$$

the Seebeck thermoelectric potential,

$$S_P(N^*, T, r_d) \equiv \int_0^T Q(N^*, T, r_d)dT, \quad (84)$$

and finally the dimensionless figure of merit,

$$ZT(N^*, T, r_d) \equiv \frac{T\times S_P^2(N^*, T, r_d)\times\sigma(N^*, T, r_d)}{K_T(N^*, T, r_d)}. \quad (85)$$

We now evaluate the above results (81-85) in the following.

In degenerate (d)-Si systems, for $N = 10^{21}\ cm^{-3}$ and in the temperature range from T=3 to 300 K, our numerical calculation indicates that: (i) the maximal value of absolute relative deviations between Q determined in Eq. (81) and its approximate form: $-C_Q \times T$ is found to be equal to 6.16×10^{-3}, and (ii) the maximal value of absolute relative deviations between T_S determined in Eq. (82) and its approximate form: $-C_S \times T$ is equal to 0.019. So, our numerical results of $Q \simeq -C_Q \times T$ and $T_S \simeq -C_S \times T$ are plotted in Figures 9b and 9c, as functions of T, respectively, suggesting that at a given T, Q and T_S both decrease with increasing r_d, due to the donor-size effect.

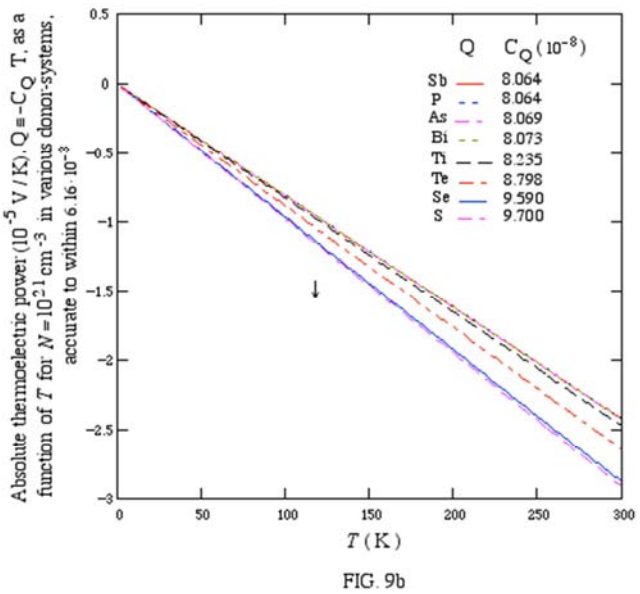

Figure 9b. *Our results of $Q \simeq -C_Q \times T$ are plotted as functions of T, suggesting that, at a given T, Q decreases with increasing r_d, due to the donor-size effect.*

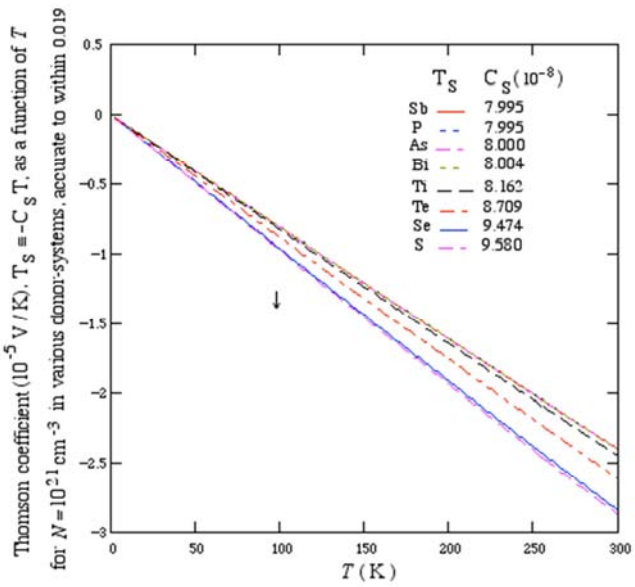

FIG. 9c

Figure 9c. *Our results of $T_S \simeq -C_S \times T$ are plotted as functions of T, suggesting that at a given T, T_S decreases with increasing r_d, due to the donor-size effect.*

Finally, in the following Figures 9d, 9e and 9f, our numerical results of Peltier coefficient P_T, Seebeck thermoelectric potential S_B, and dimensionless figure of merit ZT, calculated using Eqs. (83-85), are plotted as functions of T, respectively.

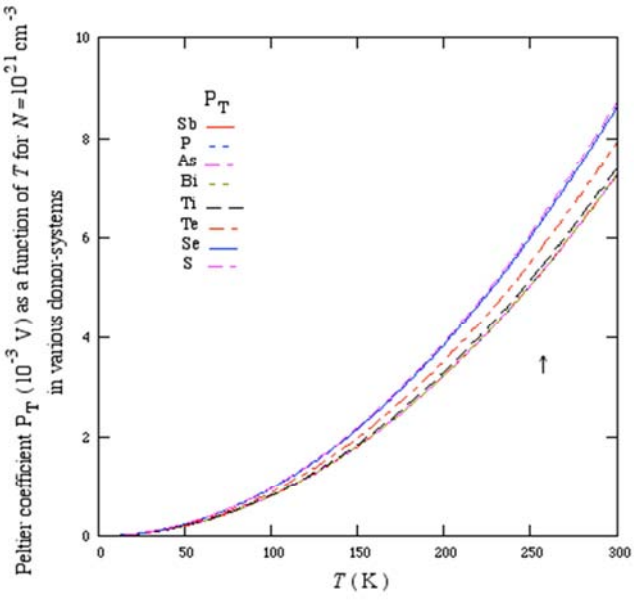

FIG. 9d

Figure 9d. *Our results of Peltier coefficient P_T are plotted as functions of T, suggesting that at a given T, P_T increases with increasing r_d, due to the donor-size effect.*

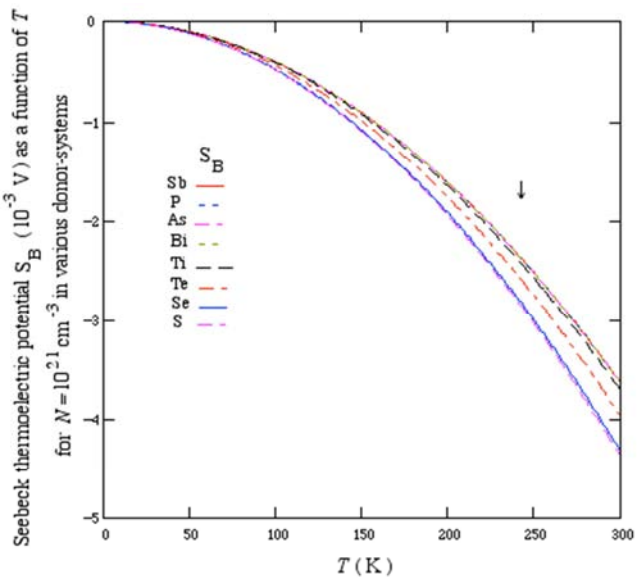

FIG. 9e

Figure 9e. *Our results of Seebeck thermoelectric potential S_B are plotted as functions of T, suggesting that at a given T, S_B decreases with increasing r_d, due to the donor-size effect.*

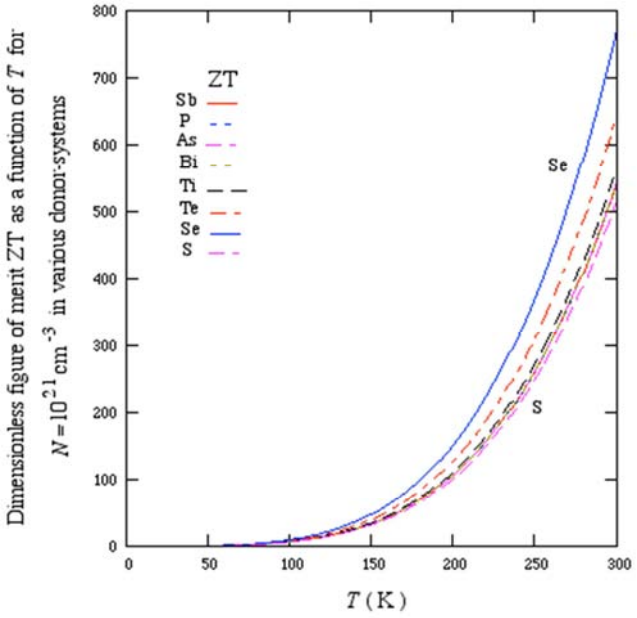

FIG. 9f

Figure 9f. *Our results of dimensionless figure of merit ZT are plotted as functions of T.*

9. Concluding Remarks

Using the effective autocorrelation function for potential fluctuations W_n, developed in Eq. (B.6) of the Appendix B, expressed in terms of the Heisenberg uncertainty relation given in Eq. (B.5), and an expression for the Gaussian average of $\mathbb{E}_k^{a-\frac{1}{2}}$, $\langle \mathbb{E}_k^{a-\frac{1}{2}} \rangle_{KIM}$, obtained in Eq. (20) by the Kane integration method (KIM), we developed the expressions for density of states, optical absorption coefficient, and electrical conductivity, obtained in various degenerate d-Si systems,

being due to the effects of donor-size and heavy doping, as given respectively in Eqs. (36, 49, 72). It should be noted that this average expression was found to be equivalent to that obtained by the Feynman path-integral method. Then, those above results were expressed in terms of $\mathbb{E}^{a-(1/2)}$, as given in Eq. (24) for $\mathbb{E} \geq 0$ and $a \geq 1$, vanished at the band edge: $\mathbb{E} = 0$, and exhibited their exponential tail behaviors for $\mathbb{E} \leq 0$, as obtained in Eqs. (28-31), in Tables 4, 7, 14, and in Figures 1, 2a (b), 3a (b, c), 4, 5a (b), 7 and 8a (b). Furthermore, in Figures 1, 4, and 7, some important conclusions were obtained as follows.

(i) First, for a given value of $-\mathbb{E}$, those exponential tails increased with increasing r_d, being due to the donor-size effect.

(ii) Secondly, they vanished at the conduction-band edge $\mathbb{E} = -0$, as given in Eq. (26), in good accordance with our other results obtained in Eq. (A3) of the Appendix A. Furthermore, those exponential tail-results were also compared with other theoretical ones, being found to be constant, at $\mathbb{E} = -0$, obtained in the small time approximation [21, 29, 30] and in the full ground-state case and deep-tail approximation [21]. Thus, their results should be not correct, as discussed in Eq. (26).

(iii) Finally, for $\mathbb{E} \leq 0$, they went to zero as $\mathbb{E} \rightarrow -0$ and $-\infty$ and presented the maxima, being found to be in good accordance with an asymptotic form for the exponential conduction-band tail, obtained by Halperin and Lax [19], using the minimum counting methods. Hence, the problem posed in the past for those exponential tails [14, 17, 19, 21, 23, 25, 29, 30, 37] should now be solved.

Then, an expression for the average of $\mathbb{E}^p$, at low temperatures and for $p \geq 3/2$, calculated by the Fermi-Dirac distribution function, was determined in Eq. (34), being used to evaluate, in degenerate d-Si systems, the mobility, conductivity, resistivity, Hall coefficient, Hall factor, Hall mobility, thermal conductivity, diffusion coefficient, absolute thermoelectric power, Thomson coefficient, Peltier coefficient, Seebeck thermoelectric potential, and finally dimensionless figure of merit, as those given in Tables 5, 6, 8-13 and 15, and in Figures 6a (b) and 9a (b, c, d, e, f), suggesting a satisfactory description for our obtained results.

In summary, the central results of the present paper were found to be:

(i) the effective autocorrelation function for potential fluctuations W_n, determined in Eq. (A9) and expressed in terms of the Heisenberg uncertainty relation given in Eq. (B.5), being also equivalent to that given in Eq. (A1) of the Appendix A,

(ii) an expression for the Gaussian average of $\mathbb{E}_k^{a-\frac{1}{2}}$ for $a \geq 1$, obtained in Eq. (20), being strongly affected by W_n, and

(iii) an expression for the average of $\mathbb{E}^p$, at low temperatures and for $p \geq 3/2$, determined in Eq. (34).

Finally, we hope that our present results could be verified by future experiments, and those given in degenerate acceptor-Si systems at low temperatures would also be investigated by a similar treatment.

Acknowledgements

The author thanks Dr. Nghi Q. Lam, Former Editor-in-Chief of Applied Physics Letters, for his helpful suggestions which have greatly improved the presentation of this paper, and also Professors: P. Aigrain, M. Balkanski, J. L. Birman, D. E. Cox, P. G. De Gennes, G. J. Dienes, J. Friedel, L. Néel, and A. Salam for their encouragements when he arrived in Paris (Orsay University) in 1979.

Appendices

Appendix A: Joint Density of States at 0 K

Friedberg and Luttinger (FL) [20] studied the behavior of the density of states $(DOS)_n$ or the joint DOS $(JDOS)_n \equiv J_n(\mathbb{E})$ for a simple method used for the n-type crystal in the limit of very low positive energies $(\mathbb{E} \rightarrow 0_+)$ by reformulating the problem conjectured by Lifshitz (L) [18] as that given in the Brownian motion. Here, they showed that $J_n(\mathbb{E} \rightarrow 0_+) \rightarrow 0$, and $J_n(\mathbb{E})$ vanishes for $\mathbb{E} \leq 0$, neglecting the exponential conduction-band tail, due to the heavy doping effect, $\mathbb{E}$ being the total electron energy. Then, these LFL results were reviewed by Mieghem [24]. In Sections III-VI, since $(DOS)_n$ given in Eq. (36) for a=1, is proportional to $\langle \mathbb{E}_k^{\frac{1}{2}} \rangle_{KIM}$, being defined in Eq. (20), we obtained: $(DOS)_n \rightarrow 0$ when $\mathbb{E} \rightarrow +0$ and -0, as discussed in Eqs. (23, 26), respectively. In other words, $(DOS)_n \rightarrow 0$, when $|\mathbb{E}| \rightarrow 0$ or $(DOS)_n$ vanishes at the conduction-band edge ($\mathbb{E} = 0$), suggesting thus a generalized (LFL)-method (GLFLM) to be study as follows.

In the very large volume $\mathbb{V}_o \equiv (\frac{4\pi}{3})\mathbb{R}_o^3$ of radius $\mathbb{R}_o$, being empty of donors, and for lowest $|\mathbb{E}| \equiv \frac{\hbar^2\pi^2}{2m_n^{HDE} \times R_o^2} \equiv \frac{\hbar^2 \times k^2}{2m_n^{HDE}}$, $\mathbb{R}_o$ is thus defined by [18, 20]

$$\mathbb{R}_o(|\nu_n|; B) \equiv \sqrt{B^2\hbar^2/(2m_n^{HDE} \times |\mathbb{E}|)} = \frac{B}{k} = \frac{B}{k_{Fn} \times \sqrt{|\nu_n|}}, \quad (A1)$$

where from the LFL-method [18, 20]: $B = B_{LFL} = \pi$ and $\mathbb{R}_o = \mathbb{R}_{o(LFL)} = \frac{B_{LFL}}{k}$, k being the wave number. Here, $m_n^{HDE}(N, r_d)$ is determined in Eq. (8), and $|\nu_n| \equiv \frac{|\mathbb{E}|}{\mathbb{E}_{Fno}}$ is determined in Eq. (21). In fact, Eq. (A1) is thus the Heisenberg uncertainty relation, which can be compared with that given in next Eq. (A8) of the Appendix B, as: $\Delta r \equiv |\vec{r} - \vec{r'}| = \frac{B_n}{k} = \frac{B_n}{k_{Fn} \times \sqrt{|\nu_n|}}$, $B_n = 2.7185$. Here, $\vec{r}$ and $\vec{r'}$ are the electron positions, according to the first-and-second scatterings at the times t and t'.

Then, using a transformation given in Eq. (48), as $a \geq 1$, Eq. (A1) thus becomes

$$\mathbb{R}_o^{GLFLM}(|\nu_n|;B) \equiv \mathbb{R}_o(|\nu_n|;B) \times \left(\frac{1}{|\nu_n|}\right)^{a-1}. \quad (A2)$$

Now, in our GLFLM, in which the very large volume is $\mathbb{V} \equiv \frac{4\pi}{3} \times \mathbb{R}^3$, $\mathbb{R} \equiv (\mathbb{R}_o^{GLFLM} - d\mathbb{R})$ being its radius, where $d\mathbb{R} \ll \mathbb{R}$, the low-lying levels for states localized in it will be insensitive to the exact conditions on the boundary $d\mathbb{V}$ of $\mathbb{V}$, and we may take the wave function to be zero on $d\mathbb{V}$. Here, one has

$$\mathbb{V} \equiv \frac{4\pi}{3} \times \mathbb{R}^3 = \frac{4\pi}{3} \times [(\mathbb{R}_o^{GLFLM})^3 - 3(\mathbb{R}_o^{GLFLM})^2 \times d\mathbb{R} + 3\mathbb{R}_o^{GLFLM} \times (d\mathbb{R})^2 - (d\mathbb{R})^3].$$

The probability of such a large region is proportional to: $\exp(-\frac{N}{g_c} \times \mathbb{V})$, where $\frac{N}{g_c} = \frac{k_{Fn}^3}{3\pi^2}$, such that the reduced J_n can be defined by: $\mathbb{h}_n^{GLFLM}(|\nu_{n(p)}|;B) \equiv \exp(-\frac{N}{g_c} \times \mathbb{V})$ [20]. Here, $d\mathbb{R}$ ($\ll \mathbb{R}$) is determined from the FL-results as [20]: $d\mathbb{R} \equiv 2c\lambda_o \simeq \lambda_o$, since $c = 0.628$ and $\lambda_o \equiv 1/\sqrt{4\pi L \times (\frac{N}{g_c})}$ is the skin depth, L being the scattering length. Moreover, in degenerate d-Si systems, the scattering length L could be replaced by the effective screening length, k_{sn}^{-1}, where k_{sn} is determined in Eq. (4). So, in this GLFLM, for lowest $|\mathbb{E}|$ (or $|\nu_n| \to 0$), defining the kinetic energy of localization by: $\mathbb{E}_{k_{sn}} \equiv \frac{\hbar^2 k_{sn}^2}{2m_n^{HDE}}$, one thus obtains

$$\ln \mathbb{h}_n^{GLFLM}(|\nu_n| \to 0;B) = -\frac{k_{Fn}^3}{3\pi^2} \times \mathbb{V} = -\frac{4B^3}{9\pi} \times |\nu_n|^{-3(a-\frac{1}{2})} + 4c \times B^2 \times \sqrt{\frac{R_{sn}}{3\pi}} \times |\nu_n|^{-2(a-\frac{1}{2})} - 4Bc^2 \times R_{sn} \times |\nu_n|^{-(a-\frac{1}{2})} +$$

$$4c^3 \times \sqrt{\frac{\pi \times R_{sn}^3}{3}} \to -\infty,\ \mathbb{h}_n^{GLFLM}(|\nu_n| \to 0;B) \to 0, \quad (A3)$$

where $R_{sn} \equiv \frac{k_{sn}}{k_{Fn}}$ is determined in Eq. (4), being in good accordance with our results (23, 26). Furthermore, for a=1 and $B = B_{LFL} = \pi$, the first-and-second terms of the last member of Eq. (A3) are found to be identical to the L-and-FL results, respectively.

Appendix B: Effective Autocorrelation Function

In degenerate d-Si systems, if denoting the electron positions and the corresponding wave vectors, according to the first-and-second scatterings at the times t and t′ by $(\vec{r}, \vec{k})$ and $(\vec{r'}, \vec{k'})$, and working with the Fourier transform given in Eq. (18), the effective autocorrelation function for potential fluctuations is then defined by [25]

$$W_n \equiv \langle V(r)V(r')\rangle = \sum_{(\vec{k},\vec{k'})} v_j(\vec{k})v_j(\vec{k'}) \times e^{i(\vec{k}.\vec{r}+\vec{k'}.\vec{r'})} \times \sum_{(j,j')} \langle e^{-i(\vec{k}.\vec{R_j}+\vec{k'}.\vec{R_{j'}})}\rangle, \quad (A4)$$

where the total potential energy $V(r)$ is defined in Eq. (16), and $i^2 = -1$. Then, since $\langle V(r)\rangle = \langle V(r')\rangle = 0$ as remarked in Eqs. (16, 17), W_n is non-zero only when $\vec{R_j} = \vec{R_{j'}}$ and $\vec{k} = -\vec{k'}$, meaning that the electron scattered on each donor twice, and giving:

$$\Delta k = |\vec{k'} - \vec{k}| = 2k. \quad (A5)$$

Hence, for $W_n(|\vec{r} - \vec{r'}|) \neq 0$, Eq. (A4) thus becomes

$$W_n(|\vec{r} - \vec{r'}|) = \mathcal{N} \sum_{\vec{k}} |v_j(\vec{k})|^2 \exp[i\,\vec{k}.(\vec{r} - \vec{r'})], \quad (A6)$$

noting that $v_j(\vec{k})v_j(\vec{k'}) = v_j(\vec{k})v_j^*(\vec{k}) = |v_j(\vec{k})|^2$ for real potential energies. Here, $v_j(\vec{k})$ is determined in Eq. (18) and $\mathcal{N}$ is the total number of donors. Further, from the Fourier transform [25], one has

$$\frac{\exp(-k_{sn} \times |\vec{r}-\vec{r'}|)}{|\vec{r}-\vec{r'}|} \equiv \sum_{\vec{k}} \frac{4\pi}{\Omega} \times \frac{1}{k^2+k_{sn}^2} \times \exp[i\,\vec{k}.(\vec{r} - \vec{r'})],$$

where Ω is the total crystal volume, and taking its partial derivative (i.e., $\partial / \partial k_{sn}$), one finally finds

$$W_n(|\vec{r} - \vec{r'}|) \equiv \eta_n^2 \exp(-k_{sn} \times |\vec{r} - \vec{r'}|). \quad (A7)$$

Here, $\eta_n^2 \equiv N \int_0^\infty v_j(r)^2 \times 4\pi r^2 dr = 2\pi N q^4 k_{sn}^{-1} \varepsilon_n^{-2}$, where -q is the electron charge, $v_j(r)$ is determined in Eq. (17) and the accurate screening length k_{sn}^{-1} is determined in Eq. (4). Then, some concluding remarks can be obtained below.

(i) In the small time approximation, $|\vec{r} - \vec{r'}| \simeq 0$, Eq. (A7) is thus reduced to η_n^2 [17, 21, 22, 29, 30].

(ii) Using Eq. (A5), the Heisenberg uncertainty relation between $\Delta r \equiv |\vec{r} - \vec{r'}|$ and $\Delta k = 2k$ is given by

$$\Delta r \times \Delta k = \mathcal{H}_n \geq 1/2 \Rightarrow \Delta r = B_n/k,\ B_n = \mathcal{H}_n/2, \quad (A8)$$

which can be compared with that given in Eq. (A1), as discussed above. Here, the values of empirical Heisenberg parameter $\mathcal{H}_n$ was proposed in Section V as: $\mathcal{H}_n$=5.4370. Futher, if replacing the constant B given in above Eqs. (A1-A3) by $B = B_n = \mathcal{H}_n/2 = 2.7185$, which gives: $B_{LFL} = \pi = 3.1416 > B_n$, then, from Eq. (A3), we also obtain: $\ln \mathbb{h}_n^{GLFLM}(|\nu_n| \to 0;B_n) \to -\infty$ or $\mathbb{h}_n^{GLFLM}(|\nu_n| \to 0;B) \to$

0, in good accordance with our results (23, 26).

(iii) Finally, using Eq. (A8) and defining the kinetic energy of localization by: $\mathbb{E}_{k_{sn}} \equiv \frac{\hbar^2 k_{sn}^2}{2m_n^{HDE}(N,r_d)}$, the effective autocorrelation function for potential fluctuations (A7) can be rewritten as

$$W_n(\nu_n, N, r_d) = \eta_n^2 \times \exp\left(\frac{-\mathcal{H}_n R_{sn}}{2\times\sqrt{|\nu_n|}}\right), \quad (A9)$$

where the ratio $R_{sn} \equiv \frac{k_{sn}}{k_{Fn}}$ is determined in Eq. (4). Here, one remarks that $W_n(\nu_n, N, r_d) \to 0$ and η_n^2, as $\nu_n \to 0$ and ∞, respectively, while in many other works for any ν_n-values, $W_n(\nu_n, N) \simeq \eta_n^2$, obtained in the small time approximation [17, 21, 22, 29, 30]: $\Delta r \simeq 0$, being only valid as $\nu_n \to \infty$, but is not correct as $\nu_n \to 0$, since from Eq. (A8), $\Delta r \gg 0$. Therefore, Eq. (A9) is an important result of the present paper.

Appendix C: Fermi Energy and Generalized Einstein Relation

The Fermi energy $\mathbb{E}_{Fn}$ and the generalized Einstein relation $\frac{D}{\mu} \equiv \frac{N}{q} \times \frac{d\mathbb{E}_{Fn}}{dN}$, which relates the diffusion coefficient D with the mobility μ, obtained for any T and N, being investigated in our previous papers, with precisions of the order of: 2.11×10^{-4} and 10^{-3}, respectively, [27, 63] are now summarized in the following.

Fermi Energy, $\mathbb{E}_{Fn}$

We first define the reduced impurity density as: $u \equiv \frac{N}{N_{CB}}$, N_{CB} being the effective density of conduction-band (CB)-states defined by: $N_{CB} = 2g_c\left(\frac{m_n^{HDE}(N,r_d)\times k_B T}{2\pi\hbar^2}\right)^{\frac{3}{2}}$ (cm^{-3}), where $m_n^{HDE}(N, r_d)$ is determined in Eq. (8). Then, for any T and N, our expression for reduced Fermi energy, θ_n, determined in our previous paper [27], is given by

$$\theta_n(u) \equiv \frac{\mathbb{E}_{Fn}(u)}{k_B T} = \frac{G(u)+Au^B F(u)}{1+Au^B},\ A = 0.0005372,\ B = 4.82842262, \quad (A10)$$

where, in the degenerate case or as $\theta_n(u \gg 1) \to \infty$, Eq. (A10) is reduced to

$$F(u) = au^{2/3}\left(1 + bu^{-4/3} + cu^{-8/3}\right)^{-2/3},\ a = \left[3\sqrt{\pi}/4\right]^{2/3},\ b = \frac{1}{8}\left(\frac{\pi}{a}\right)^2,\ c = \frac{62.3739855}{1920}\left(\frac{\pi}{a}\right)^4, \quad (A11)$$

and in the non-degenerate case or for $\theta_n(u_n \ll 1) \ll 0$, to

$$G(u) \simeq Ln(u) + 2^{-\frac{3}{2}} \times u \times e^{-du},\ d = 2^{3/2}\left[\frac{1}{\sqrt{27}} - \frac{3}{16}\right] > 0. \quad (A12)$$

Further, one notes that Eq. (A11) can thus be rewritten as

$$\mathbb{E}_{Fn1}(u) = \mathbb{E}_{Fno} \times \left(1 + bu^{-4/3} + cu^{-8/3}\right)^{-2/3}, \quad (A13)$$

being the Fermi energy given in the degenerate d-Si systems.

For example, in the degenerate P-Si system at T=77 K and $N(10^{19}\ cm^{-3}) = 3$ and 100, the relative deviations between $\mathbb{E}_{Fn1}(N^*, T, r_d)$ determined in Eq. (A13) and $\mathbb{E}_{Fn}(N^*, T, r_d) = \theta_n \times k_B T$ in Eq. (A10), defined by: $1 - \frac{\mathbb{E}_{Fn1}}{\mathbb{E}_{Fn}}$, are equal to 0.052 and 4.6×10^{-4}, respectively.

Generalized Einstein Relation

The generalized Einstein relation is defined by [51, 62-67]

$$\frac{D(u)}{\mu} \equiv \frac{N}{q} \times \frac{d\mathbb{E}_{Fn}}{dN} \equiv \frac{k_B \times T}{q} \times \left(u\frac{d\theta_n}{du}\right), \quad (A14)$$

where μ is the mobility and in particular in the degenerate case it is determined in Eq. (67), $\theta_n(u) \equiv \frac{V(u)}{W(u)}$, $V(u) = G(u) + Au^B F(u)$, and $W(u) = 1 + Au^B$ [27, 63] as those given in Eqs. (A10, A11, A12). Then, differentiating this function $\theta_n(u)$ with respect to u, one thus obtains $\frac{d\theta_n}{du}$. Therefore, Eq. (A14) becomes [63]

$$\frac{D(u)}{\mu} = \frac{k_B \times T}{q} \times u\frac{V'(u)\times W(u) - V(u)\times W'(u)}{W^2(u)}, \quad (A15)$$

where $W'(u) = ABu^{B-1}$ and $V'(u) = u^{-1} + 2^{-\frac{3}{2}}e^{-du}(1 - du) + \frac{2}{3}Au^{B-1}F(u)\left[\left(1 + \frac{3B}{2}\right) + \frac{4}{3}\times\frac{bu^{-\frac{4}{3}} + 2cu^{-\frac{8}{3}}}{1 + bu^{-\frac{4}{3}} + cu^{-\frac{8}{3}}}\right]$. One remarks that: (i) as $u \to 0$, one has: $W^2 \simeq 1$ and $u[V' \times W - V \times W'] \simeq 1$, and therefore: $\frac{D}{\mu} = \frac{k_B \times T}{q}$, and (ii) as $u \to \infty$, one has: $W^2 \approx A^2u^{2B}$ and $u[V' \times W - V \times W'] \approx \frac{2}{3}au^{2/3}A^2u^{2B}$, and therefore:

$$\frac{D(u)}{\mu} \simeq \frac{D_o(u)}{\mu} = \frac{2}{3}(\mathbb{E}_{Fn1}/q), \quad (A16)$$

where $\mathbb{E}_{Fn1}$ is determined in Eq. (A13).

Now, in the degenerate case, replacing $\mathbb{E}_{Fn}$ given in Eq. (A14) by $\mathbb{E}_{Fn1}$ determined in Eq. (A13), Eq. (A14) thus becomes

$$\frac{D_1(u)}{\mu} \approx \frac{2}{3}(\mathbb{E}_{Fn1}/q) \times \left\{1 + \frac{4}{3} \times \frac{(bu^{-4/3} + 2cu^{-8/3})}{(1 + bu^{-4/3} + cu^{-8/3})}\right\}, \quad (A17)$$

where μ is determined in Eq. (67).

For example, in the degenerate P-Si system at T=77 K and for $N(10^{19}\ cm^{-3}) = 3$ and 100, the relative deviations between $D_1(N^*, T, r_d)$ given in Eq. (A17) and $D(N^*, T, r_d)$ in Eq. (A15), defined by: $1 - \frac{D_1}{D}$, are equal to: 5×10^{-4} and -2×10^{-4}, respectively.

References

[1] R. J. Van Overstraeten, *IEEE Trans. Electron Dev.*, vol. ED-20, pp. 290-298, 1973.

[2] R. K. Jain, *Physica Status Solidi (a)*, vol. 42, 221-226, 1977.

[3] H. Van Cong and S. Brunet, *Solar Cells*, vol. 5, pp. 355-365, 1982.

[4] H. Van Cong, *Physica Status Solidi (a)*, vol. 149, pp. 619-628, 1995.

[5] H. Van Cong and G. Debiais, *Solar Energy Materials and Solar Cells*, vol. 45, pp. 385-399, 1997; H. Van Cong, *Physica Status Solidi (a)*, vol. 171, pp. 631-645, 1999.

[6] D. M. Riffe, *J. Opt. Soc. Am. B*, vol. 19, pp. 1092-1100, 2002.

[7] J. Wagner and J. A. del Alamo, *J. Appl. Phys.*, vol. 63, pp. 425-429, 1988.

[8] R. Pässler, *Phys. Rev. B*, vol. 66, p. 085201, 2002.

[9] R. Pässler, *Phys. Status Solidi B*, vol. 236, pp. 710-728, 2003.

[10] D. Yan and A. Cuevas, *J. Appl. Phys.*, vol. 114, p. 044508, 2013.

[11] H. Van Cong, S. Abide, B. Zeghmati and X. Chesneau, *Physica B*, vol. 436, pp. 130-139, 2014.

[12] H. Van Cong, *Physica B*, vol. 487, pp. 90-101, 2016.

[13] J. Binbin and S. Chihtang, *J. Semicond.*, vol. 32, p. 121002, 2011.

[14] E. O. Kane, *Phys. Rev.*, vol. 131, pp. 79-88, 1963.

[15] M. Abramowitz and I. A. Stegum, Handbook of Mathematical Functions, Dover Publications, Inc., New York, 1972; I. S. Gradshteyn and I. M. Ryzhik, Table of Integrals, Series, and Products, Academic Press, Inc., New York, 1980.

[16] R. B. Feynman and A. R. Hibbs, Quantum Mechanics and Path Integral, McGraw-Hill, New York, 1965.

[17] S. F. Edwards, *Proc. Phys. Soc.*, vol. 85, pp. 1-25, 1965.

[18] I. M. Lifshitz, *Sov. Phys. –USp.*, vol. 7, pp. 549-573, 1965 [Russian original: *Usp. Fiz. Nauk*, vol. 83, pp. 617-663, 1964].

[19] I. Halperin and M. Lax, *Phys. Rev.*, vol. 148, pp. 722-740, 1966.

[20] R. Friedberg and J. M. Luttinger, *Phys. Rev. B*, vol. 12, pp. 4460-4474, 1975.

[21] H. Van Cong, *J. Phys. Chem. Solids*, vol. 36, pp. 1237-1240, 1975.

[22] H. Van Cong, S. Charar, S. Brunet, M. Averous and J. L. Birman, *Physica Status Solidi (b)*, vol. 118, pp. 757-777, 1982; H. Van Cong, S. Brunet, S. Charar, J. L. Birman and M. Averous, *Solid State Commun.*, vol. 45, pp. 611-614, 1983.

[23] V. Sa-yakanit, W. Sritrakool, and H. R. Glyde, *Phys. Rev. B*, vol. 25, pp. 2776-2780, 1982.

[24] P. V. Mieghem, *Rev. Mod. Phys.*, vol. 64, pp. 755-793, 1982.

[25] H. Van Cong, *Il Nuovo Cimento D*, vol. 6, pp. 513-520, 1985.

[26] X. Chang and A. Izabelle, *J. Appl. Phys.*, vol. 65, pp. 2162-2164, 1989.

[27] H. Van Cong and G. Debiais, *J. Appl. Phys.*, vol. 73, pp. 1545-15463, 1993.

[28] T. H. Nguyen and S. K. O'Leary, *J. Appl. Phys.*, vol. 88, pp. 3479-3483, 2000.

[29] T. Lukes and K. T. S. Somaratna, *J. Phys. C: Solid St. Phys.*, vol. **3**, pp. 2044-2056, 1970.

[30] H. Van Cong, *Phil. Mag.*, vol. 28, pp. 983-991, 1973.

[31] J. I. Pankove, Optical Process in Semiconductors, Dover Publications, Inc., New York, 1975.

[32] H. A. Weakliem and D. Redfield, *J. Appl. Phys.*, vol. 50, pp. 1491-1493, 1979.

[33] D. E. Aspnes and A. A. Studna, *Phys. Rev. B*, vol. 27, pp. 985-1009, 1983.

[34] D. E. Aspnes, A. A. Studna, and E. Kinsbron, *Phys. Rev. B*, vol. 29, pp. 768-779, 1984.

[35] L. Vina and M. Cardona, *Phys. Rev. B*, vol. 29, pp. 6739-6751, 1984.

[36] E. D. Palik, Handbook of Optical Constants of Solids I and II, Academic Press, Inc., New York, 1985 and 1991, respectively.

[37] S. John, C. Soukoulis, M. H. Cohen, and E. N. Economou, *Phys. Rev. Lett.*, vol. 57, pp. 1777-1780, 1986.

[38] P. Lautenschlager, M. Garriga, L. Vina, and M. Cardona, *Phys. Rev. B*, vol. 36, pp. 4821-4830, 1987.

[39] F. Orapunt and S. K. O'Leary, *Solid State Commun.*, vol. 151, 411-414, 2011.

[40] A. R. Forouhi and I. Bloomer, *Phys. Rev. B*, vol. 38, pp. 1865-1874, 1988.

[41] G. E. Jr. Jellison and F. A. Modine, Appl. Phys. Lett., vol. 69, pp. 371-373, 1996.

[42] L. Ding, T. P. Chen, Y. Liu, C. Y. Ng, and S. Fung, *Phys. Rev. B*, vol. 72, p. 125419, 2005.

[43] H. Van Cong and S. Brunet, *Solid State Commun.*, vol. 58, pp. 551-554, 1986.

[44] N. K. Hon, R. Soref, and B. Jalali, *J. Appl. Phys.*, vol. 110, pp. 011301, 2011.

[45] T. Wang, N. Venkatram, J. Gosciniak, Y. Cui, G. Qian, W. Ji, and D. T. H. Tan, *Optics express*, vol. 21, 32192, 2013.

[46] L. Vivien and L. Pavesi, Handbook of Silicon Photonics, Taylor and Francis Group, LLC, New York, 2013.

[47] A. Malasi, H. Taz, M. Ehrsam, J. Goodwin, H. Garcia, and R. Kalyanaraman, *APL Photonics*, vol. 1, p. 076101, 2016.

[48] H. T. Nguyen, F. E. Rougieux, B. Mitchell, and D. Macdonald, *J. Appl. Phys.*, vol. 115, p. 043710, 2014.

[49] R. J. Jaffe, Degenerate Fermion systems, MIT 8.322 Lecture Notes: Quantum Theory II-2006, 1996.

[50] F. J. Morin and J. P. Maita, *Phys. Rev.*, vol. 96, pp. 28-35, 1954.

[51] R. Kubo, *J. Phys. Soc. Japan*, vol. 12, pp. 570-586, 1957.

[52] D. A. Greenwood, *Proc. Phys. Soc.*, vol. 71, pp. 585-596, 1958.

[53] R. A. Logan, J. F. Gilbert, and F. A. Trumbore, *J. Appl. Phys.*, vol. 32, pp. 131-132, 1961; F. Mousty, P. Ostoja, and L. Passari, *J. Appl. Phys.*, vol. 45, pp. 4576-4580, 1974.

[54] P. W. Chapman, O. N. Tufte, J. D. Zook, and D. Long, *Phys. Rev.*, vol. 34, pp. 3291-3295, 1963.

[55] J. M. Luttinger, *Phys. Rev.*, vol. 135, pp. A1505-A1514, 1964.

[56] J. Zittartz and J. S. Langer, *Phys. Rev.*, vol. 148, pp. 741-747, 1966.

[57] R. Jones, *J. Phys. C (Solid State Phys.)*, vol. 8, pp. 190-201, 1970.

[58] H. Van Cong and G. Mesnard, *Physica Status Solidi (b)*, vol. 48, pp. 293-310, 1971; vol. 49, pp. 179-189, 1972; vol. 50, pp. 53-58, 1972.

[59] M. Yussouff and J. Zittartz, *Solid State Commun.*, vol. 12, pp. 959-962, 1973.

[60] M. Finetti and A. M. Mazzone, *J. Appl. Phys.*, vol. 48, pp. 4597-4600, 1977.

[61] H. Van Cong, *Physica Status Solidi (b)*, vol. 90, pp. 401-407, 1978.

[62] P. T. Landsberg, Handbook on Semiconductors*, Volume 1,* Basic Properties of Semiconductors, Elsevier Science Publishers B. V., Amsterdam, 1992; *Eur. J. Phys.*, vol. 2, pp. 213-219, 1981.

[63] H. Van Cong and Debiais, *Solid-St. Electron.*, vol. 38, pp. 83-87, 1995.

[64] T. H. Nguyen and S. K. O'Leary, *Appl. Phys. Lett.*, vol. 83, 1998-2000, 2003; *J. Appl. Phys.*, vol. 98, p. 076102, 2005.

[65] A. Khan and A. Das, *Z. Naturforsch.*, vol. 65a, pp. 882-886, 2010; *Physica B*, vol. 405, pp. 817-821, 2010.

[66] V. Palenskis, World J. Condens. *Matt. Phys.*, vol. 4, pp. 123-133, 2014; *AIP Advances*, vol. 4, p. 047119, 2014.

[67] K. P. Ghatak, S. Bhattacharya, and D. De, Einstein Relation in Compound Semiconductors and Their Nanostructures, Springer-Verlag, Berlin, Heidelberg, 2009; K. P. Ghatak, S. Bhattacharya, S. Bhowmik, R. Benedictus, and S. Choudhury, *J. Appl. Phys.*, vol. 103, p. 094314, 2008; K. P. Ghatak and B. Mitra, *Physica Scripta.*, vol. 42, pp. 103-108, 1990.

[68] G. A. Slack, *J. Appl. Phys.*, vol. 35, pp. 3460-3466, 1964.

[69] G. D. Mahan, *J. Appl. Phys.*, vol. 66, pp. 1578-1583, 1989.